4. DURABILITY PERFORMANCE OF UHPC

4.1. OVERVIEW

The dense matrix of UHPC promotes exceptional durability properties and is arguably the biggest benefit of the material. A durable concrete enables structures to last longer, reduces the cost of maintenance and helps achieve a significantly more sustainable infrastructure. To assess the durability of UHPC, the performances of several non-proprietary blends are investigated by assessing the materials' resistance to freeze-thaw cycles, ingress of chlorides as well as the presence and distribution of air voids. The main experimental variables are cement type and the quantity of silica powder, which varies from 0% to 25% of the cement weight. All mixes display negligible chloride ion penetration and high resistance to freeze-thaw with mass loss well below the limit in over 60 cycles of freeze-thaw. Analysis of the test data indicates that the silica powder content has little influence on performance.

4.2. EXPERIMENTAL PARAMETERS

4.2.1. UHPC Mix Designs

UHPC blends from Chapter 3 identified as potential, lower cost mixes, were selected for durability testing in this chapter. Three different cements are considered, the previously mentioned White Cement, Portland Type V and the Ground Granulated Blast Furnace Slag. The last cement was selected due to its reduced cost and the known high durability of GGBS cements (Cheng, 2005). GGBS also has the added benefit of being a sustainable material as it is currently produced as a byproduct of the iron manufacturing process and therefore its use in concrete is an efficient method of recycling.

The quantity of cement and silica fume was held constant for all of the mixes, but the amount of silica powder was changed from 0% (none) to 25% of the total amount of cement. The water to cement ratio was held constant for all mixes, at 0.22 w/c. The admixture Advacast 575 high range water reducer was again used at a ratio of 1.35% to cement for all mixes. All of the blends tested in this chapter contain 1.5% smooth steel fibers by volume fraction. Particle sizes for each material can be found in Table 3-1. The chemical properties of Silica Fume and Silica Powder used in the testing are presented in Table 3-1. Additionally, the grain size distribution for the silica sand filler can be seen in Figure 3-1. Table 4-1 lists the mix constituents of the 9 mixes highlighted in this study. The naming scheme follows the same convention as in Chapter 3.

Name	White Cement Type I	Silica Fume	Silica Powder	Fiber (%)	F100	F12
W-25-25-1.5	1.00	0.25	0.25	1.50%	0.26	1.06
W-25-15-1.5	1.00	0.25	0.15	1.50%	0.29	1.14
W-25-00-1.5	1.00	0.25	0.00	1.50%	0.31	1.26
	Portland Type V					
PV-25-25-1.5	1.00	0.25	0.25	1.50%	0.26	1.05
PV-25-15-1.5	1.00	0.25	0.15	1.50%	0.28	1.14
PV-25-00-1.5	1.00	0.25	0.00	1.50%	0.31	1.26
	Type I / GGBS					
GG-25-25-1.5	1.00	0.25	0.25	1.50%	0.26	1.06
GG-25-15-1.5	1.00	0.25	0.15	1.50%	0.28	1.14
GG-25-00-1.5	1.00	0.25	0.00	1.50%	0.31	1.26

Table 4-1: Mix Proportions for tested UHPCs

4.2.2. Experimental Procedure

Freeze-Thaw Resistance

The resistance of concrete to the combined attack of de-icing salt and frost is evaluated by a modified CIF (Capillary suction, Internal damage and Freeze-thaw) test, where the surface scaling, moisture uptake and the internal damage were measured simultaneously. Cylindrical specimens of 6 inches (150 mm) in diameter and 12 inches (300 mm) in height were made. After 24±2 hours of curing the specimens were removed from the mold and submerged in tap water at 68 °F (20 °C) for 28 days. After storage in the water, the specimens were cut into rectangular prisms of 4.75 inches (120 mm) by 4.25 inches (107 mm) by 2.75 inches (70 mm). The cut section was away from the two ends of the cylinder to avoid surface in-homogeneity associated with a cast surface and is parallel to the finishing surface. After air drying at 68 °F (20 °C) and 65% relative humidity for 24 hours, the lateral surfaces of the specimens were sealed by the aluminum foil with butyl rubber. The freeze-thaw machine, as shown in Figure 4-1, contains fifteen stainless steel bowls, each containing one specimen. The specimen sits on four spacers so that the bottom test surface is in contact with the test liquid (Figure 4-2).

A freeze-thaw cycle duration is 12 hours. The temperature profile is as follows (Figure 4-3): the start temperature for the freeze-thaw test is 68 °F (20 °C); the temperature of the stainless steel bath with liquid (3% NaCl solution in this case) is lowered at a linear rate of 50 °F (10 °C) /hour for 4 hours; the specimens are kept at -68 °F (-20 °C) for 3 hours, then brought back up to room temperature at the same constant rate of 50 °F (10 °C) /hour as used for cooling; the temperature is maintained for 1 hour at 68 °F (20 °C) before the commencement of the next freeze-thaw cycle. During the one-hour isothermal period at 68 °F (20 °C), the amount of surface scaling, the

moisture uptake and the internal damage were measured after a specific number of freeze-thaw cycles. A total of two specimens were tested for each of the material parameters.

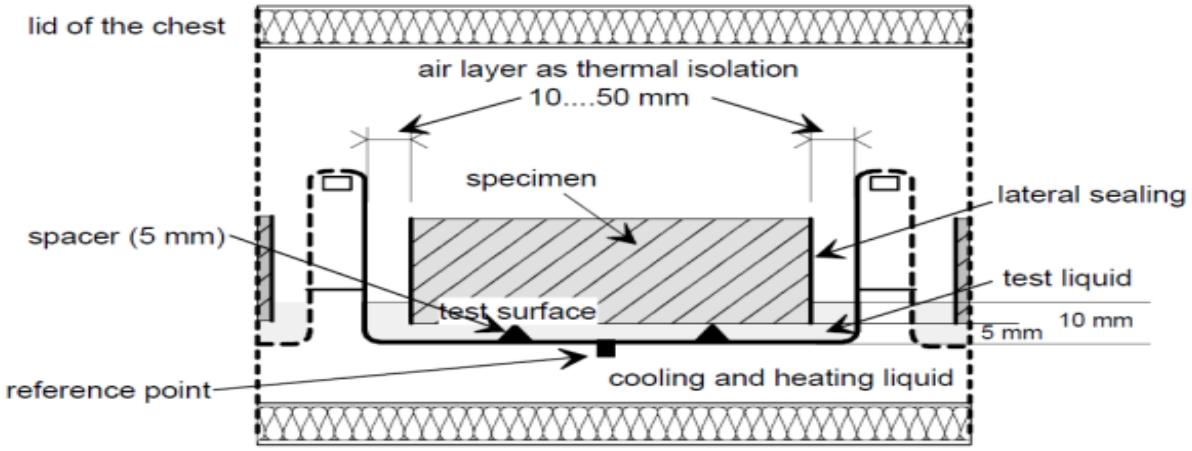

Figure 4-1: Freeze Thaw Test Close-Up (17)

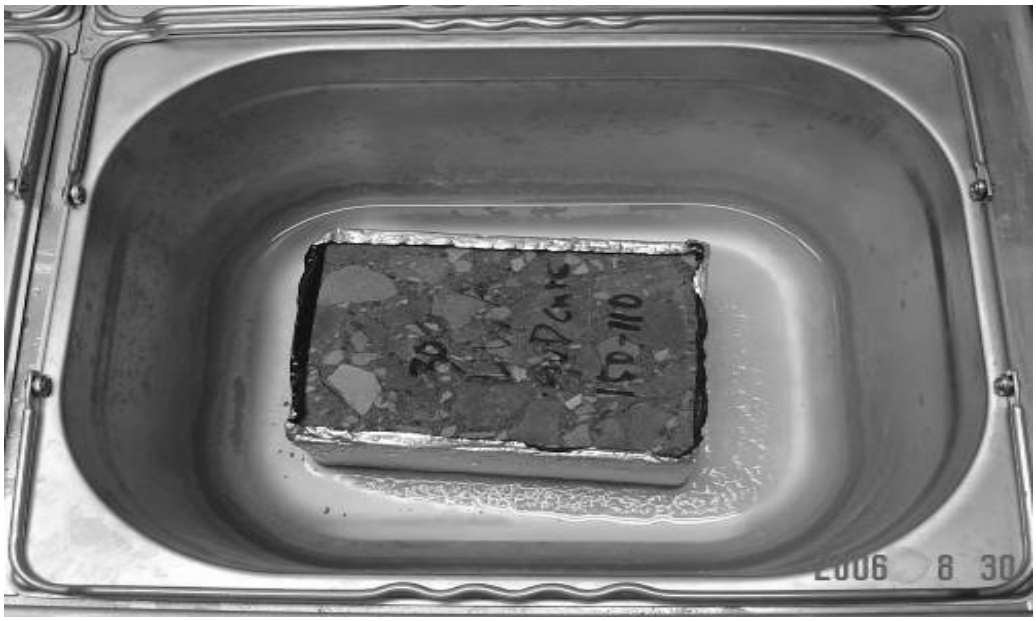

Figure 4-2: Specimen with Test Surface Facing the Bottom under Frozen Condition

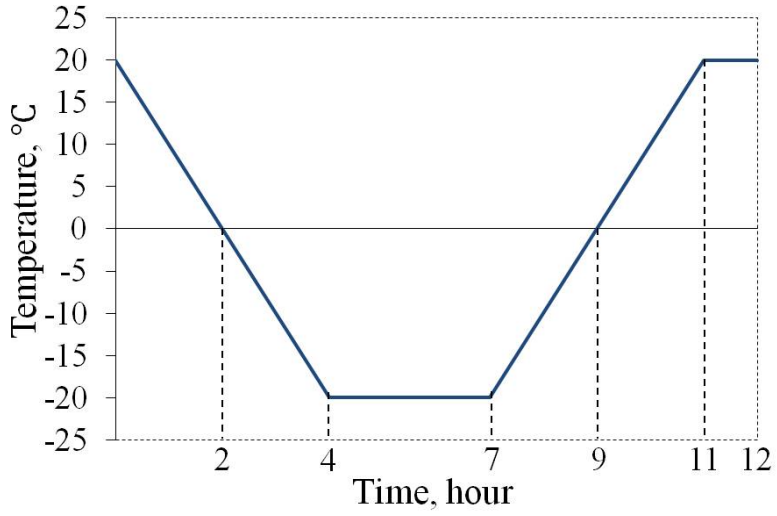

Figure 4-3: Temperature Profile of Freeze-Thaw Test

4.2.3. Air Void Analysis

The air void analysis of the concrete was measured using ASTM C457, "Standard Practice for Microscopical Determination of Parameters of the Air-Void System in Hardened Concrete". Square specimens of 4 inches (100 mm) by 4 inches (100 mm) were cut from the mid-depth portion of 6 inch (150 mm) diameter cores with the testing surface parallel to the finishing surface. Specimens were carefully polished with silicon carbide abrasives to obtain a smooth surface with undamaged paste and clearly defined air voids. Then the point count method was used to determine the fractions of air void, paste and aggregate and also the percentage of air voids with infillings. This step provides information on the quality of air void and the input to the computation of the spacing factor in the next step. After the point count procedure, the polished surface was pretreated by filling all the air voids with a white powder (barium sulfate) and the rest of the surface was darkened by a permanent marker to produce a sharp contrast (Figure 4-4). Then, the linear traverse method was used to measure the chord length distribution and the total

length of the traverse line over air void, based on which, the air void parameters can be calculated. A total of two specimens were tested for each of the material parameters.

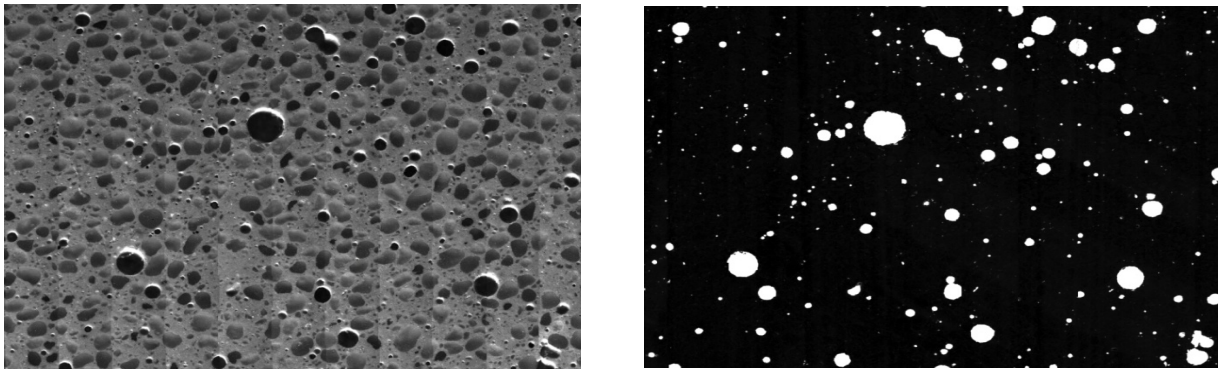

(a) Untreated Surface (b) Coated Surface

Figure 4-4: (a) Polished surface for point count measurement and (b) coated surface for linear traverse measurement.

4.2.4. Rapid Chloride Penetration Test

Evaluation of chloride ingress resistance was tested according to ASTM C1202-12, "Standard Test Method for Electrical Indication of Concrete's Ability to Resist Chloride Ion Penetration". A commercially available device, PROOVE'it, was used in order to complete the testing. Specimens of 4" (100 mm) in diameter and 2" (50 mm) in width were positioned into the measuring cell. Each cell contains a fluid reservoir at each face of the specimen. One reservoir is filled with a sodium chloride solution (3.0% NaCl). The other reservoir is filled with a sodium hydroxide solution (0.3 M NaOH).

The reservoir containing the NaCl is connected to a negatively charged terminal, the NaOH reservoir is connected to the positively charged terminal of the device's microprocessor-controlled power unit. Once started, the test automatically measures the total electrical current

passing through a concrete specimen for a standard period of 6 hours, with a direct current voltage of 60 V. A total of two specimens were tested for each of the investigated parameters.

4.2.5. Compressive Strength Testing

For each of the mixes, at least 6 cube specimens were cast. Each cube measured 2" x 2" x 2" (50 mm x 50 mm x 50 mm) and was placed into the molds without any vibration. Previous research has shown that compression test results using cubes vs. cylinders in UHPC yield 4.6 % to 6.1% higher results in the cubed specimens (Graybeal, 2006). The specimens were tested for each mix and peak compressive strength recorded. Each cube specimen was subjected to a loading rate of 0.25 kip/sec until the specimen began to strain soften in compression.

4.3. EXPERIMENTAL RESULTS

Table 4-2 shows a summary of all the test results, which are discussed in more detail in the following sections.

4.3.1. Freeze-Thaw Resistance

The freeze-thaw resistance of the ultra-high performance concrete specimens was tested in accordance with RILEM TC 176-IDC. The specimens were subjected to at least 60 freeze-thaw cycles and the mass loss of the specimens was recorded. For all of the different mixes tested, it was clear that no internal damage occurred, as evidenced by an almost unchanged relative dynamic modulus (RDM). The RDM provides a reliable measure for evaluating internal frost damage, and is calculated as follows (Equation 4-1):

$$RDM\% = \frac{n_c^2}{n^2} x100$$

Equation 4-1: Relative Dynamic Modulus

where c is the number of cycles of freezing and thawing, n_c is the resonant frequency after c cycles, and n is the initial resonant frequency (at zero cycles). For all 9 specimens, the RDM remained at 100%.

	Rapid Chloride Penetration	Air Void Analysis	Freeze-Thaw Test		Compressive Strength	
UHPC	Total Charge Passed (Coulombs)	Air Content (%)	Total Mass Loss after 28 cycles oz./yd^2 (g/m^2)		ksi (MPa)	
W-25-25-1.5	89	5.8	2.9	(98.8)	28.3	(195.0)
W-25-15-1.5	295	7.9	0.6	(20.7)	27.4	(188.8)
W-25-00-1.5	637	6.6	0.5	(17.7)	25.2	(173.6)
PV-25-25-1.5	939.5	6.1	0.5	(18.2)	25.3	(174.3)
PV-25-15-1.5	488.5	6.5	0.5	(18.0)	27.2	(187.4)
PV-25-00-1.5	57	4.5	1.2	(42.2)	25.8	(177.8)
GG-25-25-1.5	137.5	5.7	0.6	(20.5)	25.1	(172.9)
GG-25-15-1.5	229	4.8	0.7	(24.2)	26.3	(181.2)
GG-25-00-1.5	137.5	5.8	1.3	(44.7)	27.7	(190.9)

Table 4-2: Summary of Test Results

Additionally, as can be seen in Figure 4-5, mass loss for all of the specimens fell significantly below the 44.2 oz./yd^2 (1500 g/m^2) limit defined by the testing standard. This limit for mean scaling after 28 cycles measures surface scaling resistance of the specimens. For all nine specimens, this value remained consistently low, despite changes in cement types used and ratios of silica powder included. For comparison, Figure 4-5 also shows some typical results for regular concretes.

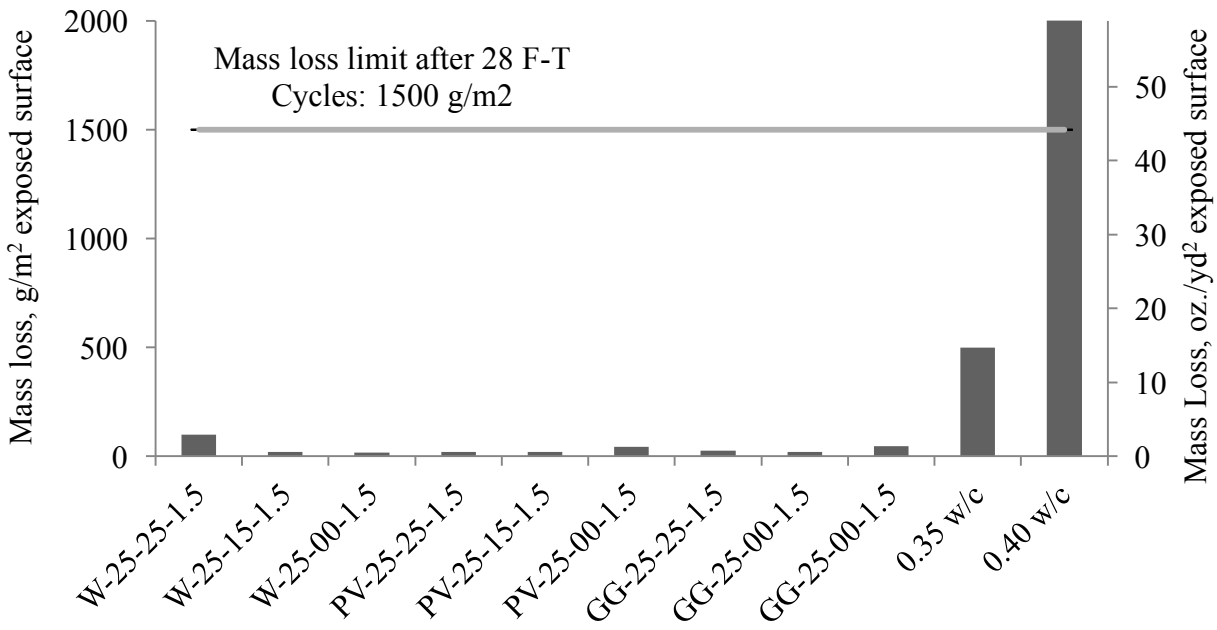

Figure 4-5: Mass Loss of UHPC Mixes after at Least 60 Cycles

From Figure 4-5, the best performing mix in terms of the least total mass loss was W-25-00-1.5, with a total loss of 0.5 oz./yd^2 (17.7 g/m^2). The worst performing mix was W-25-25-1.5, with a total loss of 2.9 oz. /yd^2 (98.8 g/m^2). Generally, there are no distinct differences in the freeze-thaw resistance of UHPCs with 0% SP, 15% SP and 25% SP. The values are all so low compared to the acceptable mass loss limits for concretes that the differences exhibited by W-25-25-1.5 are considered to be within statistical tolerances. Figure 4-5 shows that, with the exception of W-25-25-1.5, all of the mixes are within 15% of each other, and less than 3.3% of the acceptable mass losses limit for concrete, despite varying the level of silica powder and cement type.

As seen in Figure 4-6a, all specimens performed well for freeze-thaw resistance, with those containing Portland Type V performing marginally better than the other two. When averaged across all cement types, (Figure 4-6b), specimens containing 15% silica powder outperformed

those containing 25% silica powder by 40% and those containing 0% silica powder by 54%. Figure 4-7 compares the effects of cement type on the total mass loss for the UHPCs averaged for all silica powder contents. Specimens containing Portland V cement experienced 12% less mass loss than its Portland I / GGBS counterpart and 43% less mass loss than those containing white cement. Although the variations may appear large, it should be noted that all the mass loss values are small to start with and well below acceptable mass loss limits.

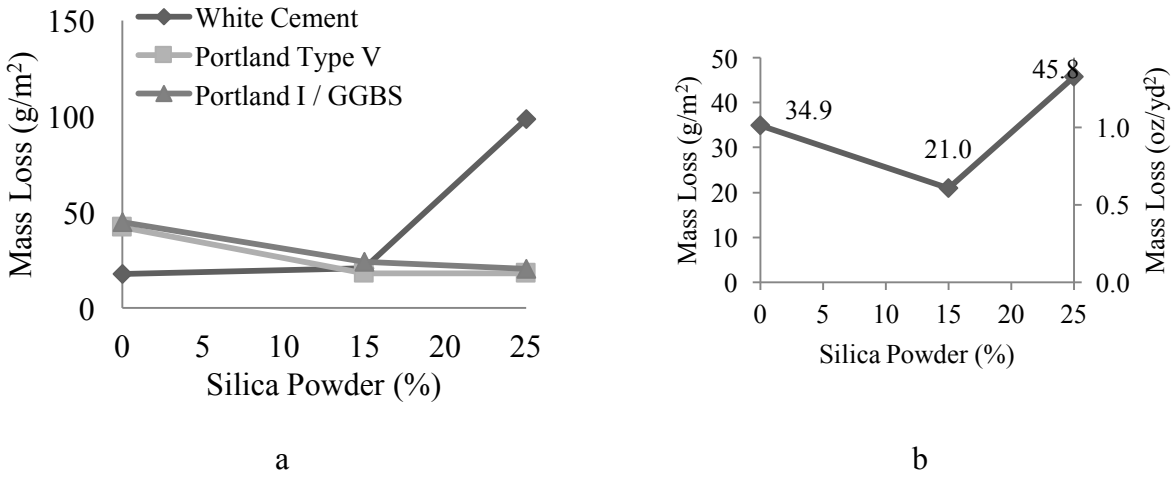

a b

Figure 4-6: a. Effect of Silica Powder on Mass Loss; b. Average Mass Loss as a Function of Silica Powder Quantity

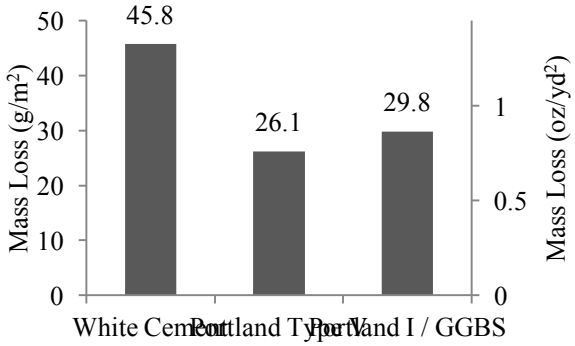

Figure 4-7: Average Mass Loss as a Function of Cement Type

4.3.2. Air Void Analysis

All of the UHPCs tested in this study tested well for freeze thaw resistance using both the linear traverse method and the point count method. The linear traverse method counts the number of voids along a single line, or chord length, while the point count method determines the number of voids within an area. Figure 4-8 shows the measured air contents using the two methods. From the chart, it can be seen that there is good agreement between the two methods.

Figure 4-8 shows that the total hardened air contents for the mixes range between 3.0% - 7.5%. These values correspond to an equivalent air content of 1.8% - 4.0% in normal concrete. Unlike regular concretes, UHPCs have a much large paste content, i.e. approximately 60% versus 30% for regular concretes. For freeze thaw, paste is the frost susceptible component, where the air-voids are embedded. In practice, air content is expressed as the air void volume as a percentage of the concrete volume. In order to accurately compare UHPC and regular concrete, the measured air content in UHPC must therefore be converted to an equivalent for regular concrete, hence the 1.8% - 4.0% range mentioned above.

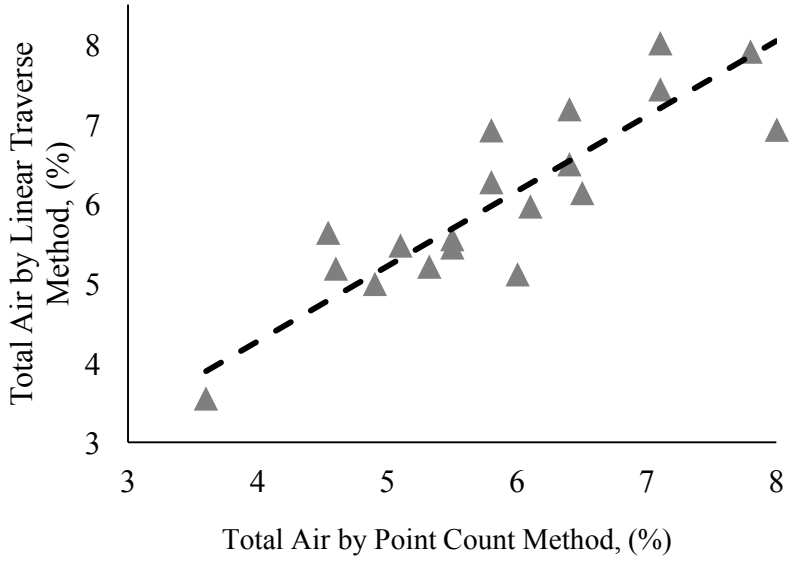

Figure 4-8: Air Content by LTM and PCM

Figure 4-9 shows the total air content as a function of the powers' spacing factor. The spacing factor here refers to the paste-void proximity; the fraction of paste within some distance of an air void. For all of the UHPC specimens tested, both air contents and spacings range from 5.9 E-4 inches to 0.02 inches (0.15 to 0.51 mm), with an average of 0.01" (0.29 mm). For normal concrete (dotted box), air-void systems with a powers spacing factor 0.0078" (0.20 mm) or less depending on conditions and 6% (+/- 1) total air content will typically provide good freeze-thaw protection (Tanesi, 2007). Though the UHPC used in this study had spacing factors higher than those of conventional concrete, it exhibited excellent freeze thaw resistance. These values also fall in line with those reported by other studies (Graybeal, 2006). Thus, the air content and/or powers spacing factor may not be a suitable metrics by which to judge the freeze-thaw resistance in UHPC.

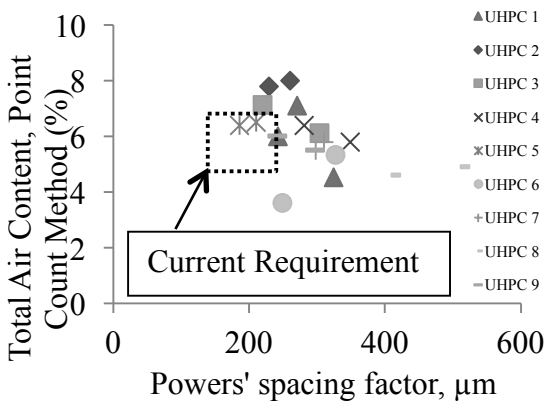

Figure 4-9: Air Content as a Function of Power's Spacing Factor

Figure 4-10a shows the air content percent as a function of silica powder for the three different cement types. The differences in air content percent between specimens containing 0%, 15% and 25% silica powder are small. When averaged across all cement types (Figure 4-10b), the air content measures are within 13% of the other specimens' air content. Figure 4-11 shows the average air content for each of the cement type used. From the data, mixes containing the Portland I / GGBS cement mix showed the least total air content percent at 5.4% when averaged across all silica powder contents. Mixes containing White cement showed air content percentages 20% higher (6.8%), and those containing Portland V cement were only 5% higher (5.7%), again when averaged across all silica contents.

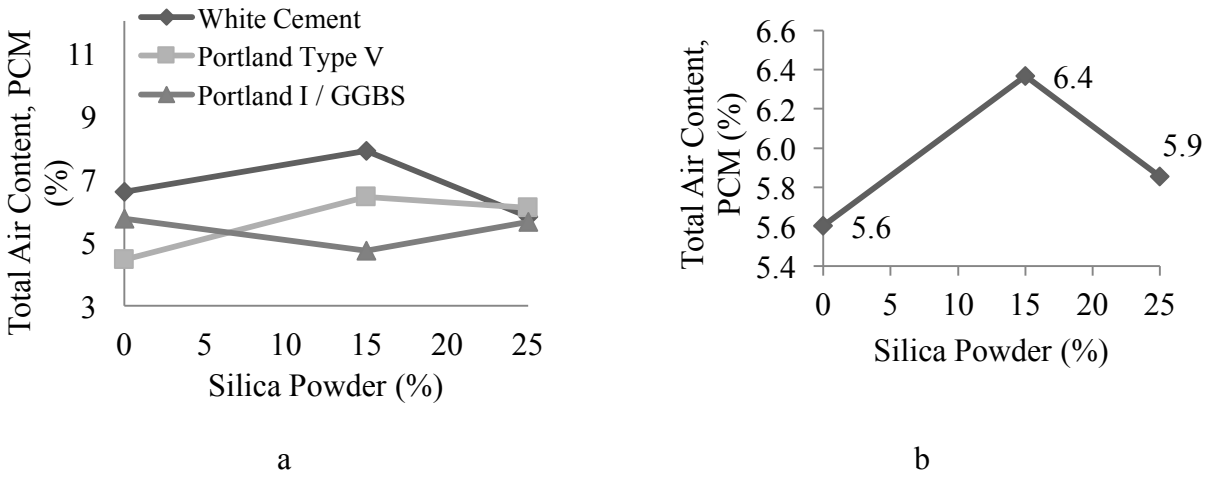

a b

Figure 4-10: a. Air Content as a Function of Silica Powder Percent, b. Average Air Content as a function of Silica Powder

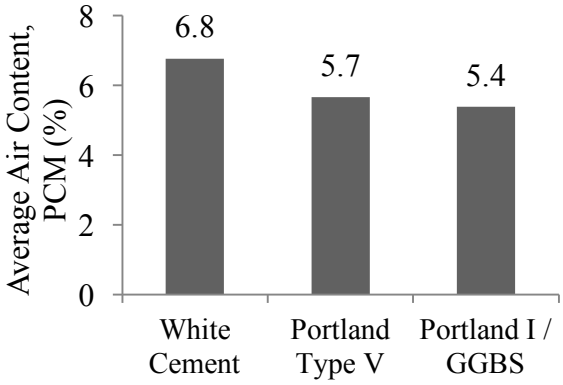

Figure 4-11: Average Air Content as a Function of Cement Type

4.3.3. Rapid Chloride Permeability

A summary of results is shown in Figure 4-12 for the nine mixes. The chloride permeability rating is illustrated based on Table 4-3. Also shown are some typical results for regular concrete.

`

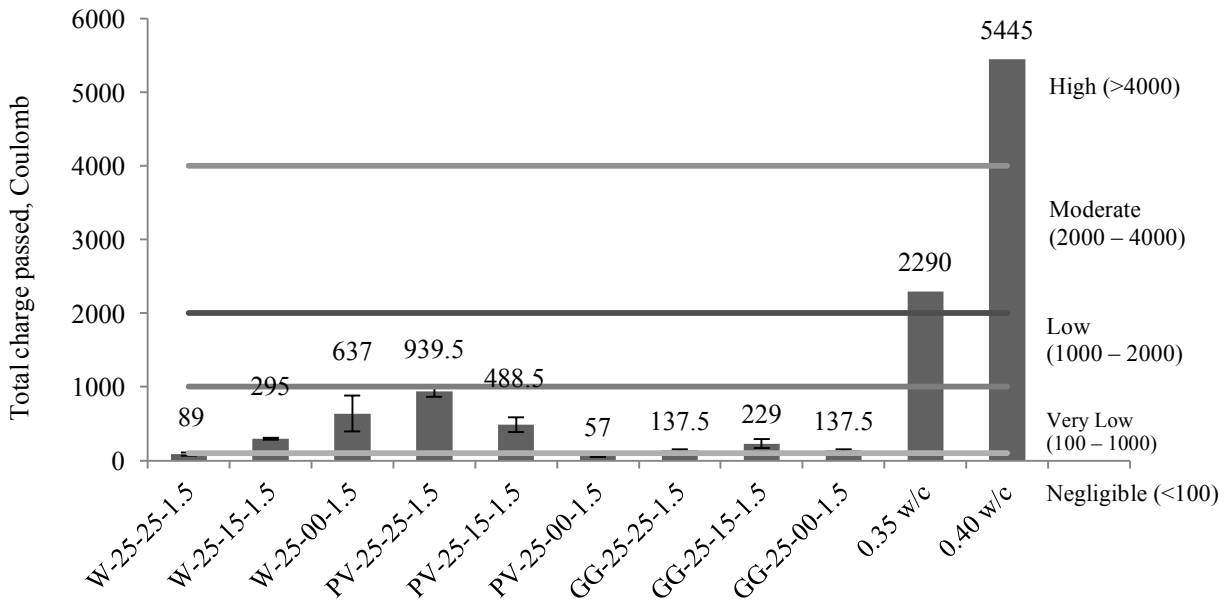

Figure 4-12: Total Charge Passed for UHP C and RC Mix

Chloride permeability	Charge (Coulomb)	Typical concrete
High	> 4000	High w/c ratio (> 0.6)
Moderate	2000 - 4000	Moderate w/c ratio (0.4 - 0.5)
Low	1000 - 2000	Low w/c ratio (< 0.4)
Very low	100 - 1000	Latex-modified concrete, internally sealed concrete
Negligible	< 100	Polymer impregnated concrete, polymer concrete

Table 4-3: Chloride Permeability Rating

From Figure 4-12, all of the UHPC mixes have a rating of "very low" chloride permeability with two mixes falling into the "negligible" category. From Figure 4-13a, it appears that the combined effect of cement type and silica powder content on the chloride ion permeability of UHPC is not clear. When averaged for all cement types, Figure 4-13b shows that the amount of silica powder

plays a role: increasing silica powder content leads to higher permeability. Specimens with 0% silica powder perform the best, averaging 277.2 coulombs passed. Those specimens outperformed ones containing 25% silica powder by 40% and those containing 15% silica powder by 17%. For comparison, regular concretes containing 35% and 40% water contents average 2073 and 4000 coulombs passed, or rather 621% and 1343% higher than the mixes containing 0% silica powder. When averaged across all silica powder contents, Figure 4-14 shows that specimens containing Portland Type I / GGBS cement exhibited the best performance on average, with all three mixes averaging 168 Coulombs passed. The mixes containing white cement averaged 340 coulombs passed, a 102% difference compared to Portland I / GGBFS. The mixes containing Portland type V averaged 495 coulombs passed, a 194% percent difference. As noted for mass loss in the freeze-thaw test results, while the variations appear large, the base values are actually small, signifying the good chloride penetration performance of all of the UHPC mixes considered.

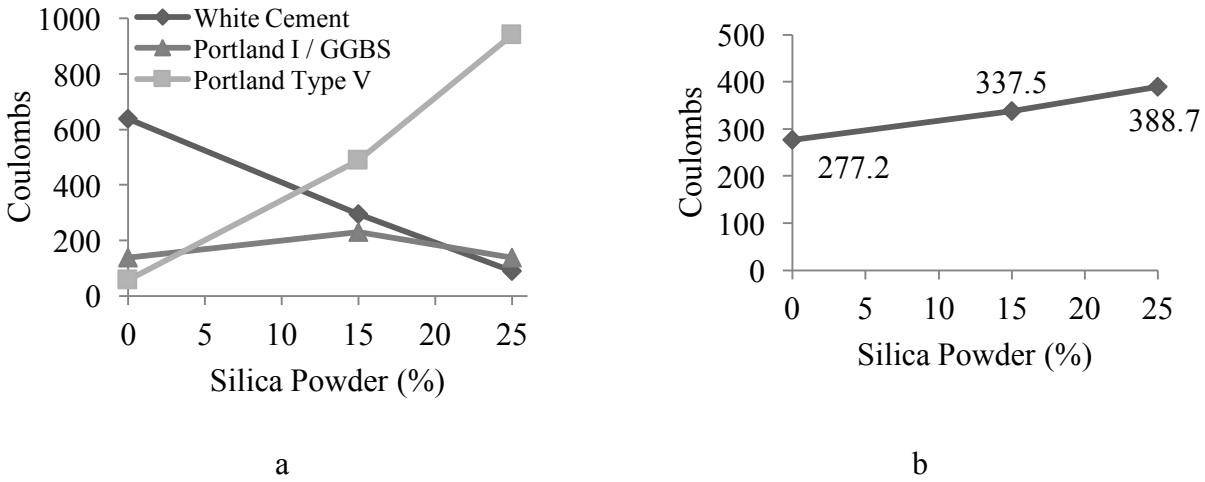

a b

Figure 4-13: a. Total Coulombs passed as a function of Silica Powder Percent; b. Average Coulombs passed as a function of Silica Powder

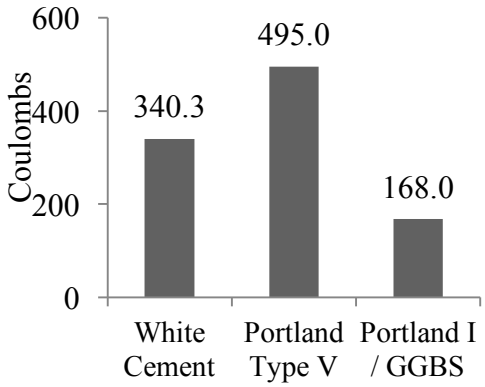

Figure 4-14: Average Coulombs passed as a function of Cement Type

4.4. DISCUSSION OF EXPERIMENTAL RESULTS

The materials tested in this research showed high durability characteristics. It is commonly accepted that the good performance of UHPC is a manifestation of the material's high packing density, which can be characterized through particle packing models. Such models consider the size and quantity of individual particulate components within a material, and show the distribution of those particles for the entire mixture. In order to achieve the densest particle packing, Andreasen and Anderson (1930) developed the Andreasen model. This paper makes use of a modified Andreasen particle packing model, as shown in equation 4-2:

$$CPFT(\%) = 100\left(\frac{d^q - d_m^q}{D^q - d_m^q}\right)$$

Equation 4-2: Modified Andreasen Model

where CPFT is equal to the cumulative percent finer than, d is the particle size for the material, d_m is the minimum particle size, D is the maximum particle size and q is the distribution coefficient. Previous studies have shown that a value of $q = 0.37$ provides higher particle packing densities for self-consolidating concretes which have similar rheology as UHPC (Brouwers, 2013). Therefore, this value was chosen for the analysis.

Figure 4-15 plots the particle size distributions for all the mixes tested in this study and compare them to the modified Andreasen model. Also plotted, for the purpose of comparison, is the distribution for regular concrete (Chia, 2002). Unlike the UHPC mixes, regular concrete deviates significantly from the ideal distribution throughout the entire range of particle sizes, suggesting that the material is sparser than UHPC. Also, regular concrete does not have any particles below 1 micron, suggesting that voids exist at this level.

Figure 4-15 shows that while variations in silica powder content affect the material's packing density differently across the particle size range; the distributions still remain close to the 'optimal' particle packing density. This provides an explanation for why there are little differences between the performances of all mixes, especially for chloride ion penetration. In essence, all the UHPCs tested in this study are so dense that they effectively resist the ingress of chloride ions. The freeze-thaw resistance in UHPCs is due to water being prevented from entering the voids. Figure 4-16 shows that all UHPCs tested had a very low water uptake percent, (<0.3% vs. approximately 1% for regular concrete (Liu, 2014)) and an unchanged RDM% indicating no internal damage.

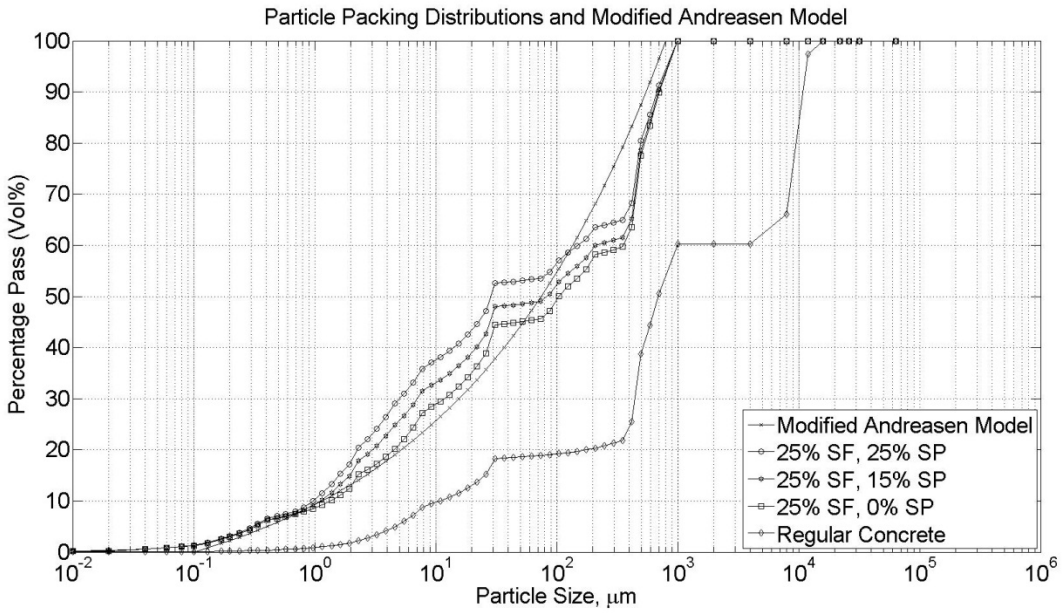

Figure 4-15: Particle Size Distributions for UHPC Mixes and Regular Concrete

One of the most important conclusions from this discussion is that silica powder has little influence on the durability of the tested UHPCs. Figure 4-15 explains why this is the case, i.e. eliminating silica powder does not significantly alter the particle size distribution. This conclusion has commercial implications because eliminating such a component from UHPC will significantly reduce its cost given the high price of silica powder, spurring widespread adoption.

Figure 4-15 also explains why changes in cement type had little effect on durability of the UHPCs tested. Each cement type had very similar particle size distributions. Thus, changes in cement type had no effect on the particle packing density of the UHPC. More work should be performed to determine the effects of cement type on other performance parameters.

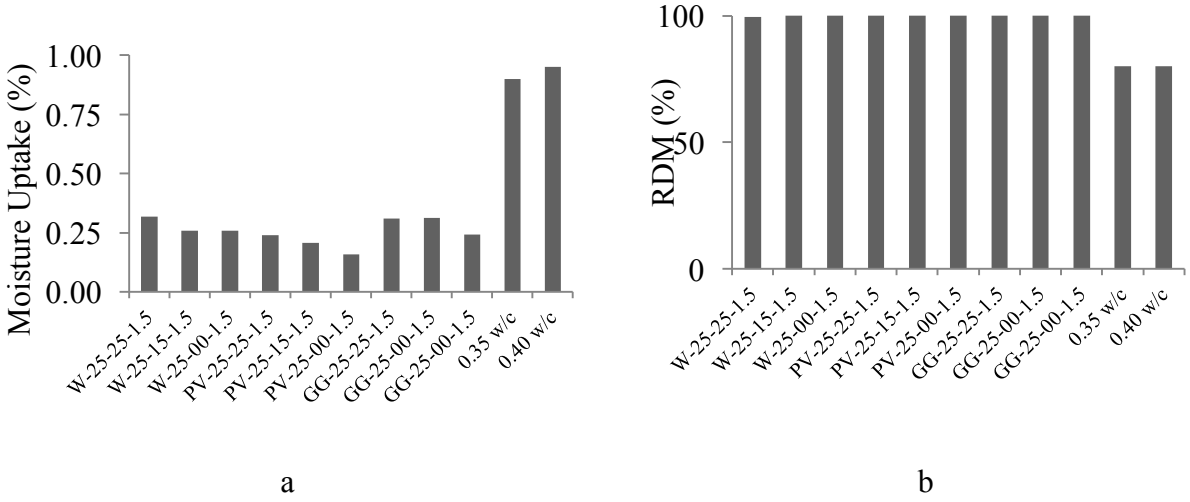

a b

Figure 4-16: Moisture Uptake and RDM% for UHPCs (27)

4.5. CONCLUSION

This experimental study investigated the durability performance of nine different blends of UHPC, including freeze-thaw resistance, chloride ion penetration resistance, and air void analysis. A modified CIF test and an air void analysis were conducted in order to evaluate freeze-thaw resistance. A rapid chloride permeability test was performed to test the concretes' resistance to the ingress of chlorides and other ions. The RDM percent change, mass loss and total air content were presented in order to gauge the concrete's freeze-thaw resistance. The coulombs passed were presented to gauge the concrete's ion permeability. The observations and findings of this study can be summarized as follows:

- All of the UHPC mixtures tested displayed exceptional resistance to freeze-thaw. All of the specimens tested experienced mass loss that was well below the mass loss limit in over 60 cycles of freeze-thaw.
- Changes in silica powder accounted for differences up to 54% mass loss in concrete's ability to withstand freeze-thaw while changes in cement type showed differences up to

43% in concrete's ability to withstand freeze-thaw. It should be noted that while the variations appear large, the absolute values on which they are based are actually small.

- The average air content for all of the specimens tested in this study ranged from 3.0% - 7.5% (1.8% - 4.0% regular concrete equivalent), below the limit for adequate resistance to freeze-thaw in regular concrete. The use of air content for assessing freeze-thaw resistance may therefore not be applicable for UHPCs. Unlike regular concrete, which relies on having sufficient void space to allow water to expand, the high freeze-thaw resistance in UHPCs is due to water being prevented from entering the material in the first place. Test results showed that all UHPCs tested had a very low water uptake percent and an unchanged RDM%, signifying no internal damage. This corresponds well to other studies of similar materials with dense matrices and shows that this phenomenon also occurs in UHPC.
- All of the UHPC mixtures show high resistance to chloride ion penetration. Concretes made with the Portland Type I / GGBS Cement blend showed the least permeability, followed by specimens made with white cement and Portland type V cement. Concretes containing silica powder at 25% showed slightly higher ion permeability than those with 15% silica powder. The least permeable concrete mixes had 0% silica powder.
- Particle size distribution studies showed that while variations in silica powder content affect the material's packing density differently across the particle size range, the resulting distributions still remain close to the optimal particle packing density. Test results confirm this observation and show that variations in silica powder content had little effect on the durability performance of the tested UHPC mixes. This signifies that this mix component could potentially be eliminated to reduce cost. Studies in Chapter 3

confirm that that elimination of silica powder, which is a key part of proprietary mixes, does not significantly influence the short term mechanical properties of the material.

5. FACTORS AFFECTING BAR BOND DEVELOPMENT FOR UHPC

5.1. OVERVIEW

While UHPC's tensile and compression behaviors are relatively well understood, an in-depth analysis of UHPC's behavior at the component level, specifically the bonding ability between UHPC and steel bar reinforcement is lacking and the meager published data is contradictory. In the study presented in this chapter, a series of tests was performed in order to characterize the bond relationship of a non-proprietary UHPC blend with steel bar reinforcement. A series of bar pull out tests were conducted using plain and epoxy-coated grade 60 bars with nominal sizes of #4, #5 and #6 (13 mm, 16 mm, and 19 mm). Other experimental parameters include three development lengths (2", 3" and 4"), two fiber orientations (longitudinal and transverse to the steel bar), two steel fiber volume contents (1% and 2%) and bond strength at early age curing (1, 3 and 7 days). Additionally, the results of four flexure bending tests using UHPC lap spliced joints (discussed in more detail in Chapter 6) were compared to the pull out results in order to determine the bond capacity in a realistic loading scenario. Results from pull out testing show that bonding stress capacity decreases with increased embedment length suggesting a non-uniform distribution of bond stresses. Bond capacity in lap-spliced joints was less than in simple pull out tests, but within current design limits for regular reinforced concrete.

5.2. EXPERIMENTAL PARAMETERS AND PROCEDURE:

5.2.1. Bar Pull Out Testing Program and Test Set Up

The simple bar pull out test is the most widely used measure of bond capacity in concrete due to its simplicity and ease of implementation. It is also considered to be the least accurate testing

method as this test method tends to overestimate the bond capacity (6). With this set up, when the steel bar is placed into tension, the surrounding concrete is placed into compression. This in turn causes compressive struts to form between the supports and the surface of the bar, placing the bar surface and bearings under compression. Unlike real structures, the surface's compressive forces are caused by the load application, and not the relative movement between the concrete and the bar. In order to minimize this effect during the testing, a modified method of supporting the concrete was implemented (Figure 5-1a).

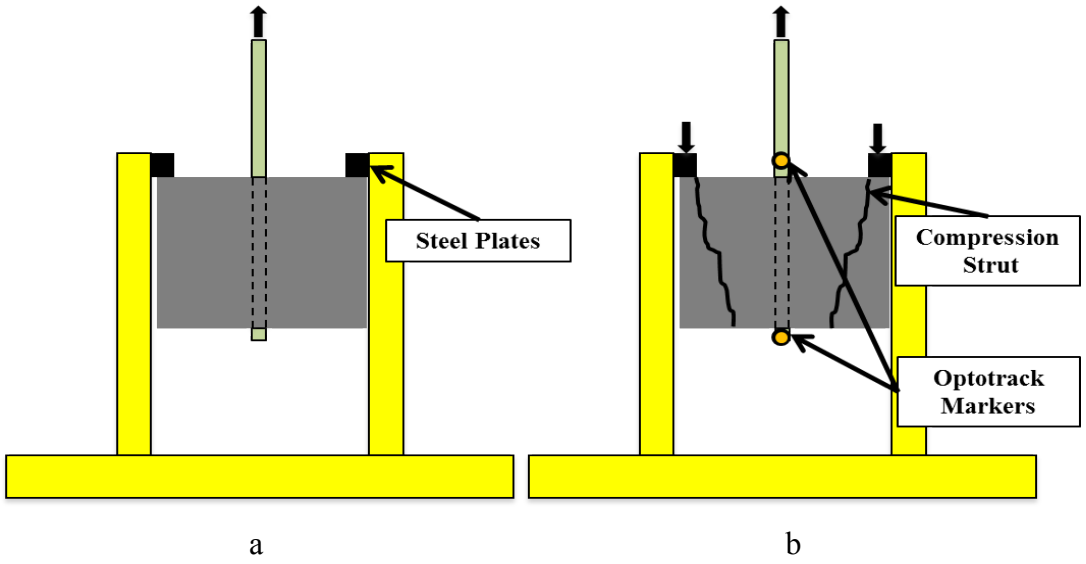

Figure 5-1: (a) Test Set Up for Bar Pull Out (b) and Instrumentation and Load Path for Specimen

Unlike the traditional bar pull out case where the entire surface of the concrete is used as a support, the new method makes use of the high bearing strength of the UHPC to minimize the surface area needed. The new configuration uses 4 small square plates, with an area of 0.5 in^2 (13 mm^2) to support the specimen. Each support was placed 2.75" (70 mm) away from the steel bar, distancing the concrete surrounding the bar from any compressive struts which may form during

loading. Specimens were subjected to a quasi-static displacement controlled load, using a 100 kip Instron hydraulic machine, at a rate of 0.001 in/sec (0.025 mm/sec). Force applied on the specimen was recorded using a 100-kip load cell. Slip in the bar was recorded using the Optotrack displacement tracking system (Figure 5-1b), which is a non-contact measurement system that employs infrared markers.

This series of tests investigated the effects of several parameters on the bonding between the UHPC and the steel bars. As shown in Table 5-1, three different bar diameters were tested at #4, #5 and #6 (13 mm, 16 mm and 19 mm), for both plain and epoxy coated bars. Each of the bars was subjected to embedment lengths of 2", 3" and 4" (50 mm, 75 mm and 100 mm). Additionally, two different bar sizes were used to investigate the differences caused by fiber alignment during casting. Specimens were casted with fibers preferentially aligned parallel with the bar and transversely to the bar (Figure 5-2). Two different bar types were used to evaluate the effect of fiber content at 1% and 2% by volume. Finally, UHPC specimens were casted and tested at 1, 3 and 7 days cured in order to determine the early age bonding ability of the material.

The naming convention for the tests performed is as follows: the first entry represents the bar size and coating (black bars or epoxy coated), followed by the embedded length in mm, the fiber volume percentage, the casting orientation (P for parallel or T for transverse) and the age of the UHPC (1, 3, 7 or 28 days). For example, 13B-100-2%-P-28D represents a #4 (13 mm) diameter plain black bar, embedded 4" (100 mm), with 2% fibers by volume, UHPC casted parallel to the steel reinforcement at 28 days.

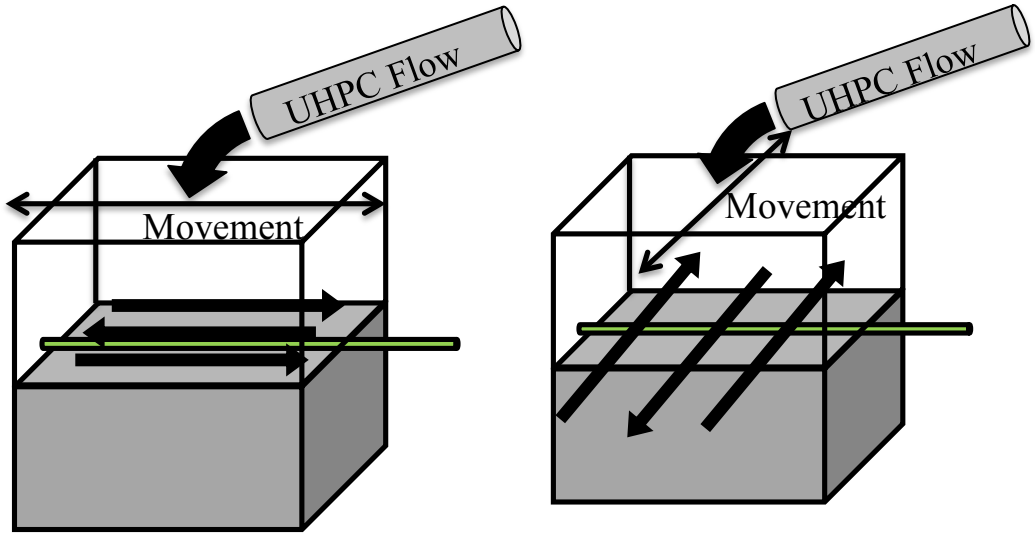

a b

Figure 5-2: (a) Fibers Aligned Parallel to Bar (b) Fibers Aligned Transversely to Bar

Name	# of Tests	Bar Diameter (mm)	Coating	Embedment Length inches (mm)	Fiber Content (% vol.)	Casting Orientation	Curing Age (days)
13B-100-2%-P-28D	2	#4 (13)	None	4” (100)	2.0%	Parallel	28
13E-100-2%-P-28D	2	#4 (13)	Epoxy	4” (100)	2.0%	Parallel	28
13B-75-2%-P-28D	2	#4 (13)	None	3” (75)	2.0%	Parallel	28
13E-75-2%-P-28D	2	#4 (13)	Epoxy	3” (75)	2.0%	Parallel	28
13B-50-2%-P-28D	2	#4 (13)	None	2” (50)	2.0%	Parallel	28
13E-50-2%-P-28D	2	#4 (13)	Epoxy	2” (50)	2.0%	Parallel	28
16B-100-2%-P-28D	3	#5 (16)	None	4” (100)	2.0%	Parallel	28
16E-100-2%-P-28D	3	#5 (16)	Epoxy	4” (100)	2.0%	Parallel	28
16B-75-2%-P-28D	2	#5 (16)	None	3” (75)	2.0%	Parallel	28
16E-75-2%-P-28D	2	#5 (16)	Epoxy	3” (75)	2.0%	Parallel	28
16B-50-2%-P-28D	2	#5 (16)	None	2” (50)	2.0%	Parallel	28
16E-50-2%-P-28D	2	#5 (16)	Epoxy	2” (50)	2.0%	Parallel	28
19B-100-2%-P-28D	2	#6 (19)	None	4” (100)	2.0%	Parallel	28

Name	# of Tests	Bar Diameter (mm)	Coating	Embedment Length inches (mm)	Fiber Content (% vol.)	Casting Orientation	Curing Age (days)
19E-100-2%-P-28D	2	#6 (19)	Epoxy	4” (100)	2.0%	Parallel	28
19B-75-2%-P-28D	2	#6 (19)	None	3” (75)	2.0%	Parallel	28
19E-75-2%-P-28D	2	#6 (19)	Epoxy	3” (75)	2.0%	Parallel	28
19B-50-2%-P-28D	2	#6 (19)	None	2” (50)	2.0%	Parallel	28
19E-50-2%-P-28D	2	#6 (19)	Epoxy	2” (50)	2.0%	Parallel	28
19B-75-1%-P-28D	2	#6 (19)	None	3” (75)	1.0%	Parallel	28
19E-75-2%-T-28D	2	#6 (19)	Epoxy	3” (75)	2.0%	Trans.	28
16E-100-2%-P-1D	2	#5 (16)	Epoxy	4” (100)	2.0%	Parallel	1
16E-100-2%-P-3D	2	#5 (16)	Epoxy	4” (100)	2.0%	Parallel	3
16E-100-2%-P-7D	2	#5 (16)	Epoxy	4” (100)	2.0%	Parallel	7
16B-100-2%-T-	3	#5 (16)	None	4” (100)	2.0%	Trans.	28
16E-100-1%-P-28D	3	#5 (16)	Epoxy	4” (100)	1.0%	Parallel	28
16E-100-2%-P-28D	3	#5 (16)	Epoxy	4” (100)	2.0%	Parallel	28

Table 5-1: Experimental Parameters and Number of Tests

5.2.2. Lap Splice Joint Testing Program

Beam specimens F-100-1P-1, F-100-1P-2, F-100-2P-1 and F-100-2P-2 described in Chapter 6 represent a more realistic anchorage scenario for UHPC. As discussed later on in Chapter 6, these specimens comprise two regular precast concrete beam elements joined together at the center with a UHPC closure pour. Bottom bars are subjected to pull out in a lap splice configuration when the beams are subjected to flexural loading. The difference between pull out and lap splice testing configurations has been understood for regular concrete for some time. ACI Committee 318-05, Section 12.15.2 (and AASHTO LFRD 5.11.5.3.1) recommends

multiplying the required anchorage length by 1.3 l_d when designing a non-contact lap splice vs. simple bar pull out for regular concrete.

Some details from Chapter 6 are repeated here for the sake of readability. Full details are found in Chapter 6. Figure 5-3 shows the construction and reinforcement details for the specimen. Longitudinal bars were spaced at 6.3" (160 mm) and transverse bars were spaced at 8" (200 mm). The lower layer of reinforcement sat at a depth of 3.3" (85 mm) (measured from the top surface) while the upper layer was placed at a depth of 1.4" (36 mm). All reinforcement consisted of epoxy-coated bars with a diameter of 16 mm (#5 bars). The UHPC joint measured 4" (100 mm) wide with a lap splice length of 3.6" (90 mm). All tests were subjected to four-point bending as shown in Figure 5-4. The UHPC joint was cast in order to favor orientation of the steel fibers parallel to the reinforcement bar direction. Force in the steel bars was computed from a cracked section analysis at the joint face.

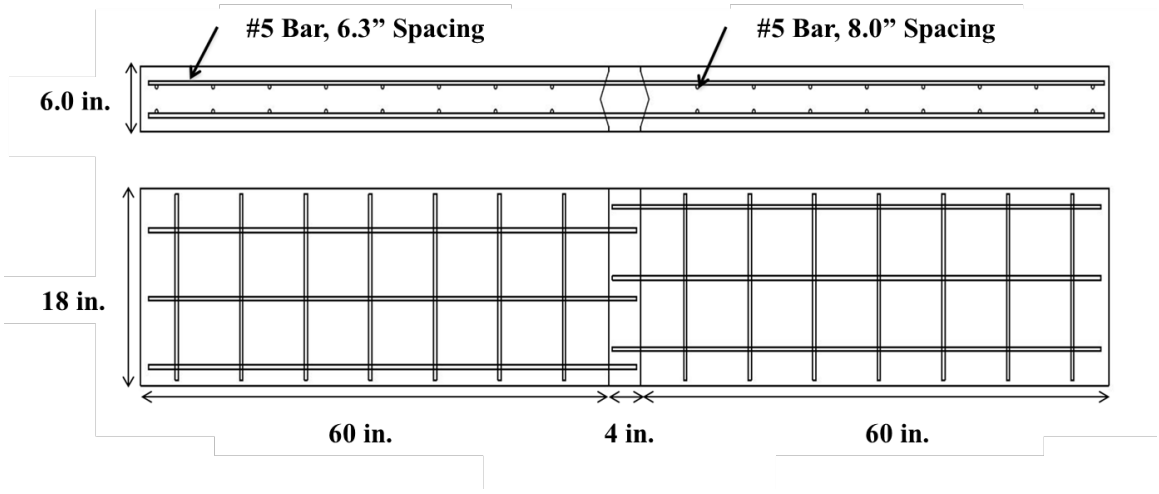

Figure 5-3: Construction and Reinforcement Details for Precast Decks with UHPC Joint

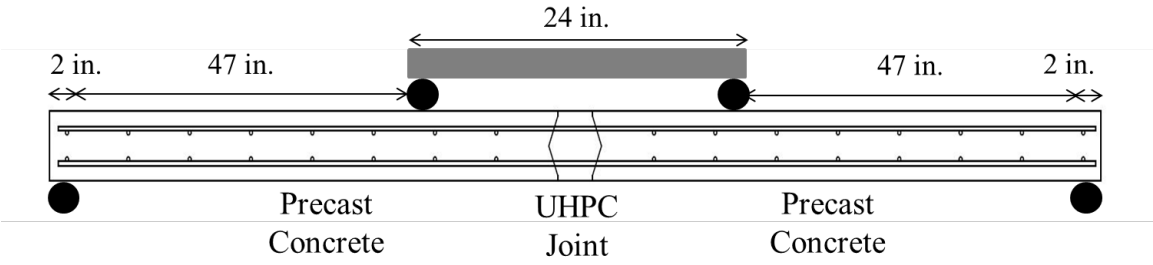

Figure 5-4: Four Point Bending Test Set Up for Flexure Test for Specimens F-100-1P-1, F-100-1P-2, F-100-2P-1 and F-100-2P-2

As discussed in Chapter 6, the beams were subjected to a displacement controlled, quasi-static load at a rate of 0.001 in/sec (0.025 mm/sec), using a 100 kip Instron hydraulic machine. Force on the specimen was recorded using a 100-kip load cell. Deformation in the UHPC joint was recorded using the Optotrack tracking system on one face of the specimen and through Digital Image Correlation on the other face.

5.2.3. Material Properties

The precast concrete beam elements were constructed using 35 MPa (5000 psi) concrete. Slump was controlled at <6" (150 mm) with a maximum aggregate diameter of 0.8" (20 mm). All steel reinforcement bars were grade 60 steel. The UHPC joint and the pull out cubes were constructed using mix GG-25-00 outlined in Chapter 3. For the simple bar pull out tests, all UHPCs consisting of 2% steel fibers by volume achieved an average 28-day compressive strength of 27.7 ksi (190.9 MPa) and 26.1 ksi (180.1 MPa) for UHPCs containing 1% steel fibers by volume. For the lap spliced joint tests, UHPCs achieved a 28 day average compressive strength of 27.9 ksi (192.36 MPa) at 2% steel fibers by volume and 26.4 (182.71 MPa) at 1% steel fibers. The regular concrete used in precast beams averaged a 28 day compressive strength of 5.25 ksi (36.23 MPa). The steel fibers are plain, smooth fibers (unlike the brass coated fibers used in

chapters 3 and 4). Each fiber is 0.75” (19 mm) long with a diameter of 0.0078” (0.2 mm) and minimum tensile strength of 285 ksi (1965 MPa).

RESULTS AND DISCUSSION

5.2.4. Bar Pull Out Results

Table **5-2** below shows the data from the bar pull out testing and lists the type of failure mode for each specimen. Testing revealed three distinct failure modes for bond (Figure 5-5); bar fracture of the steel reinforcement, slip of the bar from the UHPC, and a conical shaped failure in which the UHPC attached to the bar separates from the UHPC in the remaining cube. Data on force and bond stress are listed for the peak load at these failures. Bond stress is computed as the achieved pull out force divided by the initial surface area of the embedded portion of the bar.

(a) (b) (c)

Figure 5-5: (a) Bar Fracture, (b) Bar Slip, and (c) Conical Concrete Failure

Name	Mode of Failure			Bar Force Failure (kips)			Bond at Failure (ksi)		
	Test 1	Test 2	Test 3	Test 1	Test 2	Test 3	Test 1	Test 2	Test 3
13B-100-2%-P-28D	Fracture	Fracture	-	17.5	17.6	-	2.8	2.8	-
13E-100-2%-P-28D	Fracture	Fracture	-	17.5	17.6	-	2.8	2.8	-
13B-75-2%-P-28D	Fracture	Yield, Slip	-	15.7	14.9	-	3.3	3.1	-
13E-75-2%-P-28D	Fracture	Yield, Slip	-	16.1	15.6	-	3.4	3.3	-
13B-50-2%-P-28D	Slip	Yield, Slip	-	14.9	15.3	-	4.7	4.9	-
13E-50-2%-P-28D	Slip	Slip	-	13.8	12.0	-	4.4	3.8	-
16B-100-2%-P-28D	Slip	Slip	Slip	18.3	17.5	23.8	2.3	2.2	3.0
16E-100-2%-P-28D	Slip	Slip	Slip	18.5	20.9	22.0	2.4	2.7	2.8
16B-75-2%-P-28D	Slip	Slip	-	16.0	14.2	-	2.7	2.4	-
16E-75-2%-P-28D	Slip	Slip	-	15.5	17.0	-	2.6	2.9	-
16B-50-2%-P-28D	Slip	Slip	-	17.6	17.7	-	4.5	4.5	-
16E-50-2%-P-28D	Slip	Slip	-	17.6	18.0	-	4.5	4.6	-
19B-100-2%-P-28D	Slip	Slip	-	19.8	19.6	-	2.1	2.1	-
19E-100-2%-P-28D	Slip	Slip	-	20.1	20.8	-	2.1	2.2	-
19B-75-2%-P-28D	Cone	Cone	-	19.1	16.9	-	2.7	2.4	-
19E-75-2%-P-28D	Cone	Cone	-	21.7	17.3	-	3.1	2.5	-
19B-50-2%-P-28D	Cone	Cone	-	13.7	17.6	-	2.9	3.7	-
19E-50-2%-P-28D	Cone	Cone	-	18.0	13.7	-	3.8	2.9	-
19B-75-1%-P-28D	Slip	Slip	-	10.7	11.9	-	1.5	1.7	-
19E-75-2%-T-28D	Slip	Slip	-	15.6	16.5	-	2.1	2.2	-
16E-100-2%-P-1D	Slip	Slip	-	12.7	11.1	-	1.6	1.4	-
16E-100-2%-P-3D	Slip	Slip	-	13.6	12.7	-	1.7	1.6	-
16E-100-2%-P-7D	Slip	Slip	-	16.9	18.6	-	1.9	2.3	-
16B-100-2%-T-28D	Slip	Slip	Slip	20.6	21.0	21.4	2.6	2.7	2.7
16E-100-1%-P-28D	Slip	Slip	Slip	16.0	17.0	17.7	2.0	2.1	2.2
16E-100-2%-P-28D	Slip	Slip	Slip	17.6	21.2	21.7	2.2	2.7	2.7

Table 5-2: Test Results for Simple Bar Pull Out

5.2.5. Effect of Embedment Length

Figure 5-6 shows the effects of embedment length force-slip relation for a #4 (13 mm) dia. bar subjected to simple bar pull out. At 4" (100 mm) embedment (Figure 5-6a), all specimens failed via bar fracture, with no difference between black and epoxy coated bars. At an embedment of 3" (75 mm) (Figure 5-6b), the specimens failed in either bar fracture, or bar yielding, followed by slip in the bar. Again, differences between plain and epoxy bars were minor. At 2" (50 mm) embedment (Figure 5-6c), only one specimen yielded, followed by bar slip. The remaining specimens all experienced pure slip. At 2" (50 mm), the differences between the black and epoxy bars were more apparent, with black bars achieving a higher pull out force, and higher bond stresses. Increased ductility seen in Figure 5-6a and Figure 5-6b compared to Figure 5-6c is a result of the steel yielding prior to failure.

Figure 5-6d plots the bond stresses measured vs. embedment. As seen, when embedment was increased, the bond stresses decreased, almost linearly. This suggests that an uneven distribution of bond stresses occurs along the length of the bar. In general, three mechanisms provide resistance against the pull out of reinforcing bars; chemical adhesion, friction and the mechanical interaction between the concrete and steel. As load is applied to the specimens, chemical and frictional resistances are quickly overcome thus making the mechanical interaction the predominant resistance mechanism. Figure 5-7 shows an idealization of the reaction forces experienced by the reinforcing steel. The horizontal component of this force is referred to as the shear force. The vertical component of the bearing force creates a radial force that is responsible for splitting in the surrounding concrete.

In regular concretes, the pull out force is resisted uniformly along the length of the embedded portion of the bar (Azizinamini, 1993). In the case of high strength concretes, at low axial load

levels, the ribs closest to the loading point come into contact with concrete first, applying a bearing force to the concrete. As the load continues to increase, the bearing force increases, and the next closest rib also begin to resist the applied load. The increased bearing capacity of the concrete inhibits crushing of the concrete in the vicinity of the ribs, and thus the radial component of the force from the bearing force promotes splitting in the surrounding concrete. By the time the ultimate load is reached due to the splitting, all ribs may not be participating in resisting the load, requiring then that the first few ribs contribute the most, i.e. the bond resistance is non-uniform along the length.

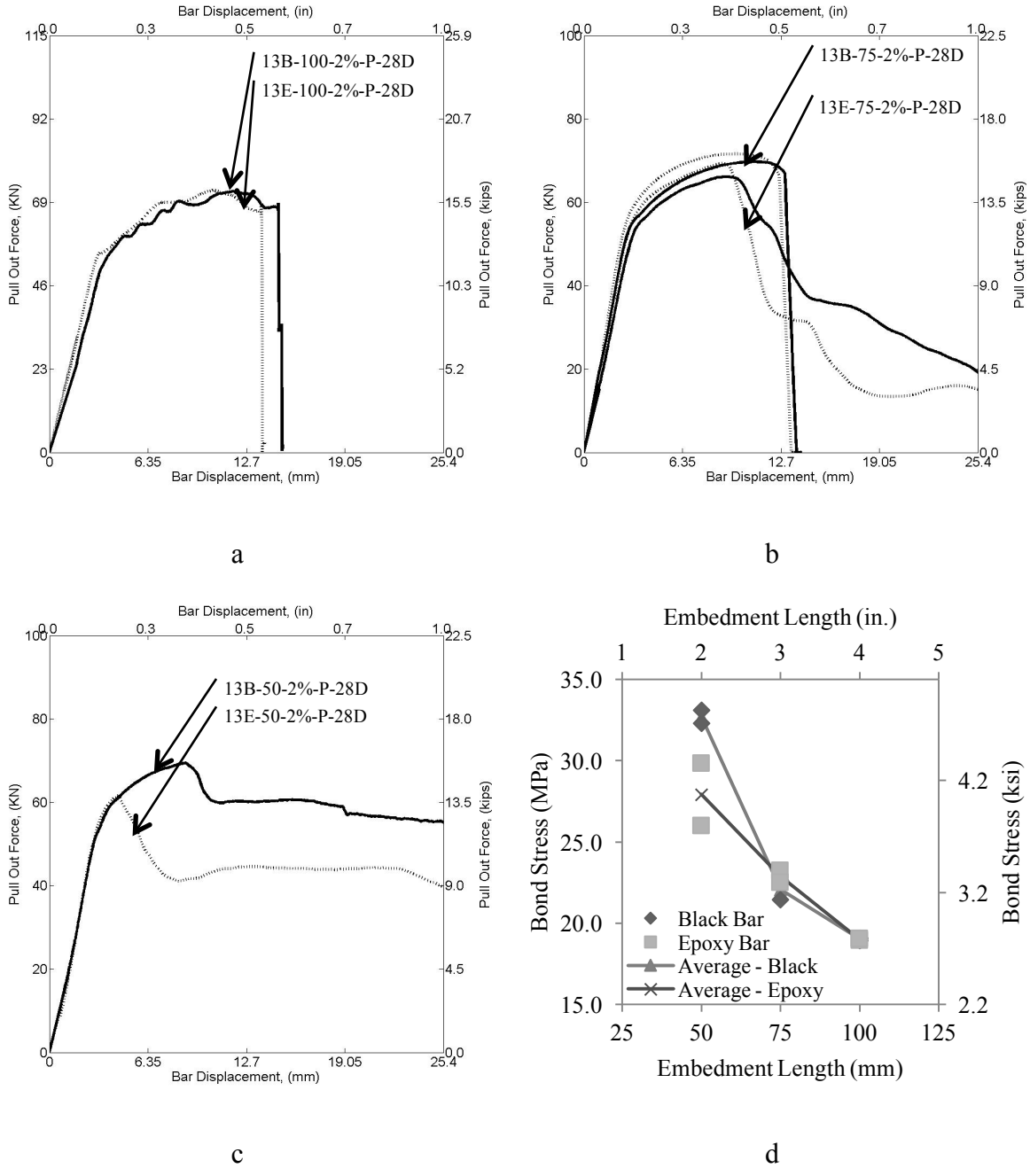

Figure 5-6: Force Slip for 13 mm bars at (a) 100 mm, (b) 75 mm, and (c) 50 mm embedment, (d) Peak Bond Stress vs. Embedment Length

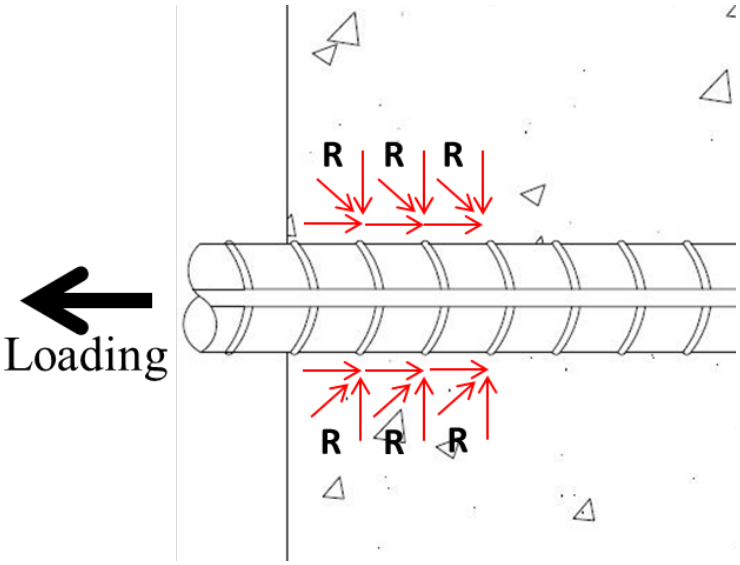

Figure 5-7: Idealized Reaction of Reinforcing Steel Embedded in Concrete, Subjected to Tension, Cross Sectional View

Figure 5-8 shows the results of embedment for #5 (16 mm) dia. bars. Unlike the #4 (13 mm) dia. bar, no #5 bars reached bar fracture. All of the specimens failed via bar slip. At 4" (100 mm), black bars were able to reach a slightly higher bond stress vs. their epoxy counter parts. This also occurred at 2" (50 mm), though at 3" (75 mm) there was no discernible difference. Again, for bar types, the total average bond stress recorded decreased with increasing embedment length. This again is attributed to the uneven force distribution along the length of the bar.

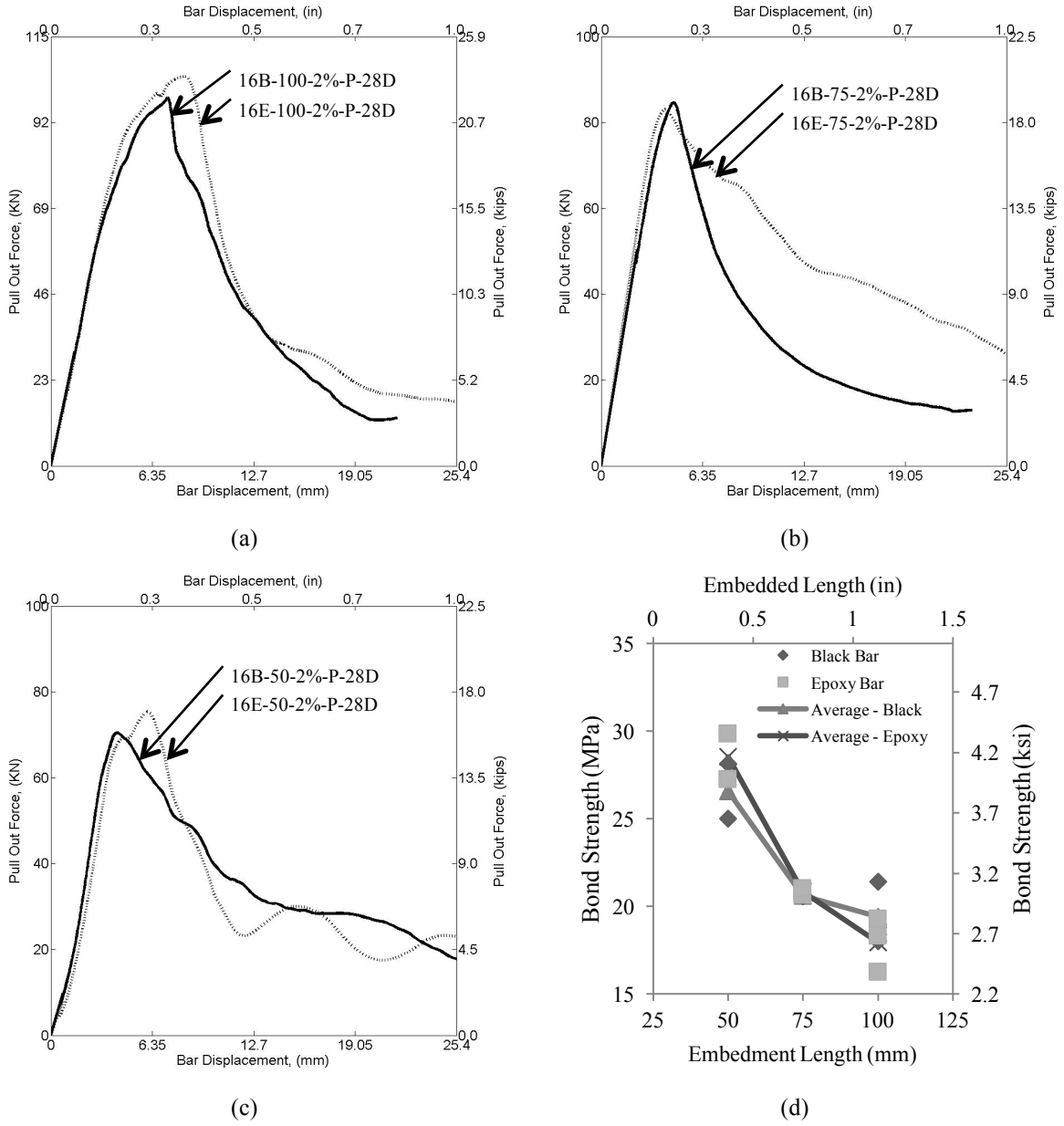

Figure 5-8: Force Slip for 16 mm bars at (a) 100 mm, (b) 75 mm, and (c) 50 mm embedment, (d) Peak Bond Stress vs. Embedment Length

Figure 5-9 shows the data for #6 (19.0 mm) dia. bars. At 4" (100 mm), all of the bars experienced slip. At 3" (75 mm) and 2" (50 mm), specimens all failed due to a conical separation in the concrete. The UHPC bonded to the bar separated from the UHPC in the cube, leading to a drop in strength. As the main failure was a tensile failure in the concrete, specimens that

experienced a cone failure showed no discernible differences between the black and epoxy coated bars. Also, as seen with the previous bar diameters, as embedment increases, the overall bond stress decreases.

The data collected on embedment from the current study differs from those reported by others. Figure 5-10a shows the bond stress data available for a #5 epoxy coated bar from previous works by Graybeal and the data collected from this study. The Graybeal bond data from the 2014 bond report (2014) shows a linear increase in the bond stress capacity with increased embedment length. However, the current study shows an opposite trend at the lower embedment lengths; increased bond stress with decreased embedment. As previously stated, the reported trend suggests that the bond development along the length of the steel bar in UHPC is non-uniform and has been observed in fiber reinforced concretes in the past (Azizinamini, 1993). In fiber reinforced concretes, the increased compressive strength delays crushing in the area surrounding the steel ribs, promoting instead splitting cracks in the surrounding concrete. As noted earlier, the ribs deeper in the embedded region may not resist the applied axial loading prior to cracking in the UHPC, and therefore the first few ribs carry the highest loads. The report by Graybeal makes mention of this phenomena, but suggests its effect may not be present in UHPC, whereas data collected from this study seems to confirm this event. Additionally, a separate Graybeal report from 2010 lists a much higher bond stress, close to 14.5 ksi (100 MPa) at a 4” (100 mm) embedment length. While some of these variations can be attributed to the test method selected (the 2014 study uses lap splices, while the 2010 study makes use of UHPC cylinders and the current study used UHPC cubes. Also both Graybeal reports use Ductal.), there are still significant differences and more work should be done here to further understand the bonding of UHPCs, especially at lower embedment lengths.

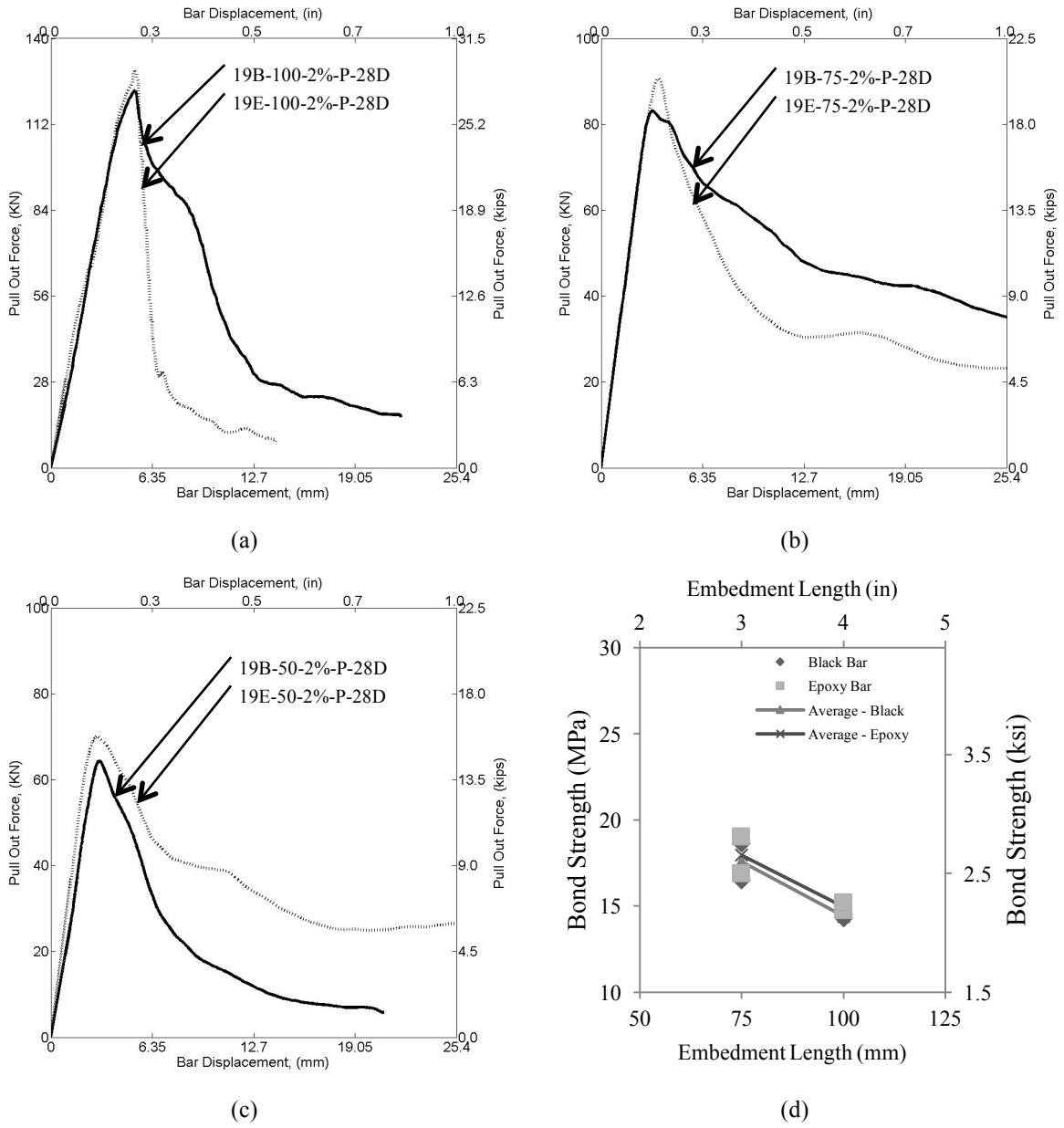

Figure 5-9: Force Slip for 19 mm bars at (a) 100 mm, (b) 75 mm, and (c) 50 mm embedment, (d) Peak Bond Stress vs. Embedment Length

Additionally, Figure 5-10 shows the reported bond values for the bar sizes tested in this study along with all other published data found by the authors. From the scatter, it is difficult to discern a clear trend, which again highlights the high variability in the reported literature. For those unspecified, bar coating used for testing was unclear.

5.2.6. Effect UHPC Cast Orientation on Bond

The effect of casting orientation and fiber alignment on bond was also investigated. Figure 5-11a shows the resulting relation for specimens with UHPC cast parallel and transversely to the steel reinforcement for a #5 (16 mm) bar. As seen, there is little difference in the achieved strengths. For the #6 (19 mm) bars, fibers aligned parallel with the bar provide a somewhat higher force resistance than those transverse to the steel bar, which leads to a 17 % difference in the peak bond stresses reached (Figure 5-11b). A closer examination of Table 5-3 shows that these differences are within the statistical range of variations in the data, and are more likely due to other factors (number of ribs embedded, etc.).

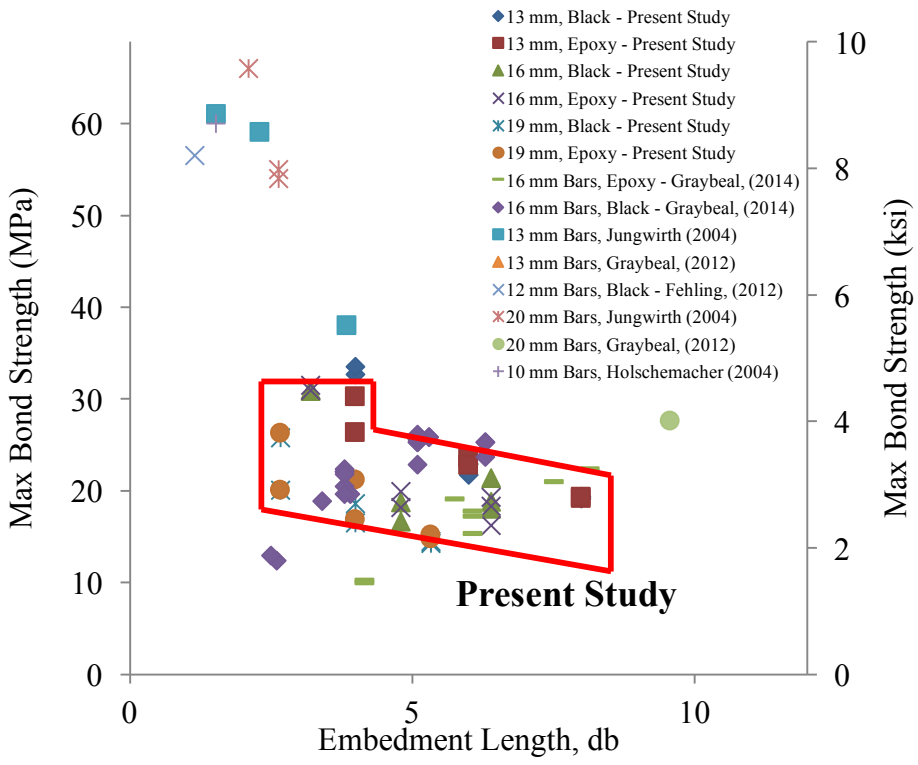

Figure 5-10: Scatter of the current data available for 13 mm, 16 mm, and 19 mm bars

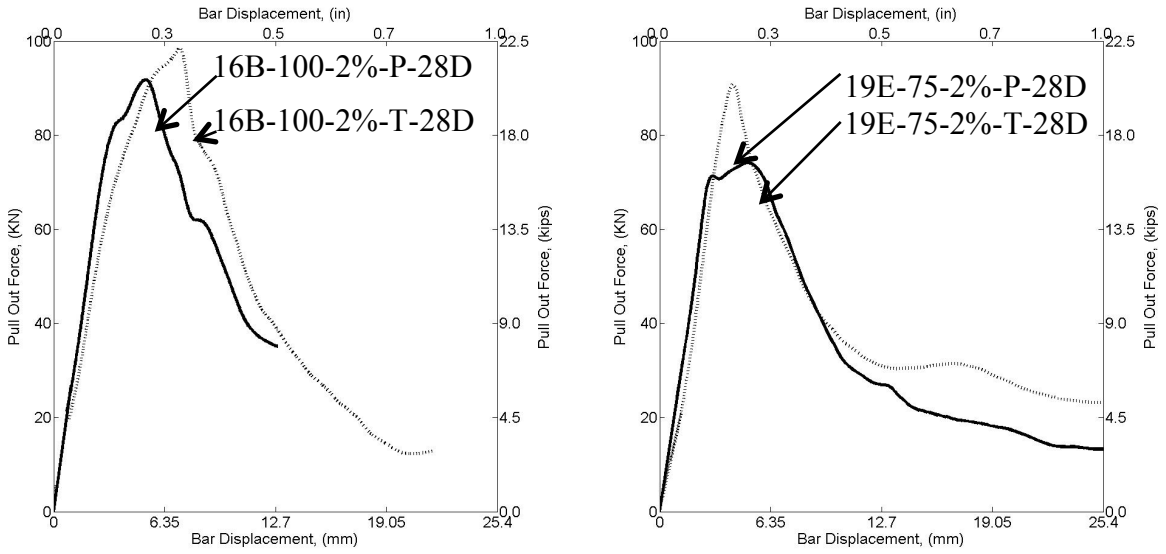

a b

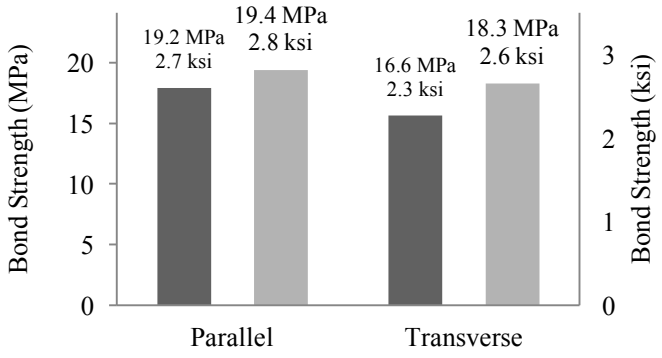

c

Figure 5-11: (a) Force Slip for 16mm bars with Parallel and Transverse Fibers, (b) Force Slip for 19 mm bars with Parallel and Transverse Fibers, and (c) Bond Stress Comparison (Dark Gray- 19 mm bars, Light Gray – 16 mm bars)

5.2.7. Effects of Fiber Volume Content

Two series of bar pull out tests were tested containing 1% fibers by volume and compared to those tested containing 2% fibers by volume. Figure 5-12a shows the two sets of force-slip relations for 16 mm bar specimens at 1% and 2% fibers by volume. The specimens containing only 1% fibers developed 21% less force than those with 2% fibers. Bond stresses saw a similar reduction in strength. For the #6 (19 mm) bar specimens (Figure 5-12b), specimens containing only 1% fibers developed 36% less force than those with 2% fibers, again with similar reductions in bond stress. The larger drop in strength for the #6 (19 mm) bar is most likely due to differences in the number of ribs embedded from specimen to specimen. More testing should be performed to determine if the reduction in strength is lower with longer embedment at different fiber contents. Figure 5-12c shows the bond stresses compared for the two fiber contents. Averaging all 5 tests, average bond strength dropped 28% from specimens with 2% fibers by volume to 1% fibers by volume. Less fiber percentage by volume translates to fewer fibers

bridging any cracks that may form during testing. This in turn reduces the confinement in the concrete, increases crack openings, and lowers slip resistance.

5.2.8. Early Age Testing of UHPC on Bond

An investigation into the bonding strength between UHPC and steel reinforcement was also performed at 1, 3 and 7 days cure time. From Figure 5-13a and Figure 5-13b, testing at 1 day generally yielded the lowest load strength and bond stress increasing at 3, 7 and 28 days respectively. Comparing Figures Figure 5-13c and Figure 5-13d, the compressive strength of the UHPC and the maximum bond stress achieved both increase asymptotically over the course of 28 days. Regular concrete follows a similar increase in early age strength vs. time which results from the pozzolonic reaction of the cement. As the UHPC uses the same cement found in regular concrete, a similar increase in strength over time is expected as the reaction requires time to complete. Similarly, as the pozzolonic reaction continues, the bonding between the cementitious material and the steel fibers strengthens. Enhanced fiber-concrete composite behavior increases the total confinement available in the UHPC, which increases the bond strength. Also, the composite achieves approximately 75% of its pull-out strength after 7 days.

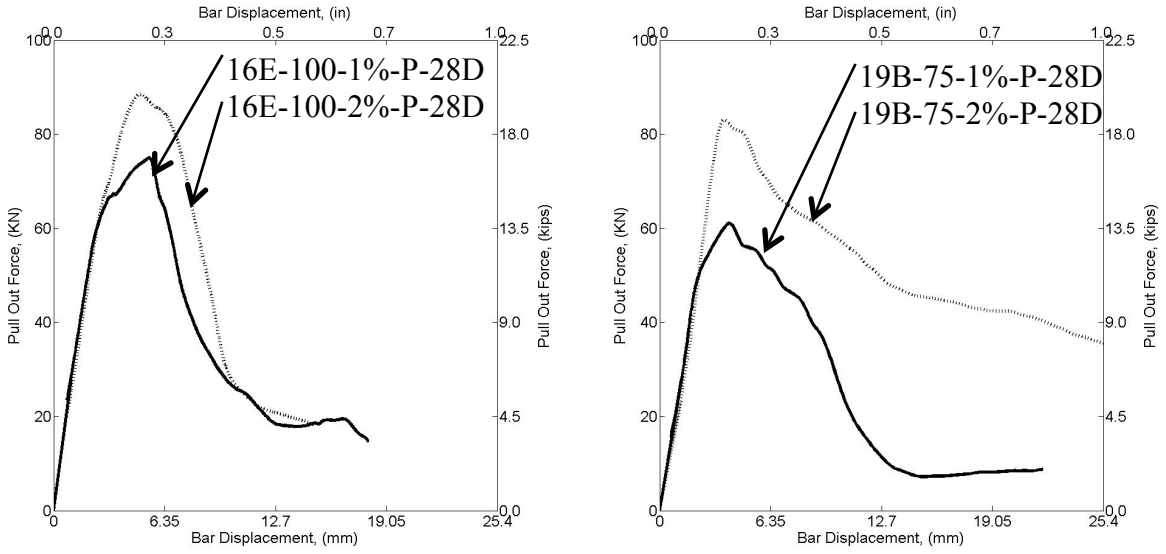

a b

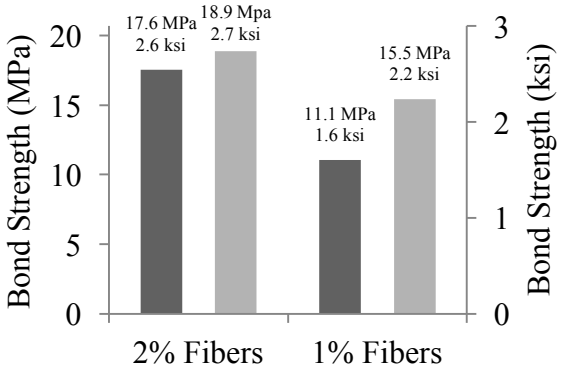

c

Figure 5-12: (a) Force Slip for 16 mm bars with 1% and 2% Fibers, (b) Force Slip for 19 mm bars with 1% and 2% Fibers, and (c) Bond Stress Comparison (Dark Gray – 19 mm bars, Light Gray – 16 mm bars)

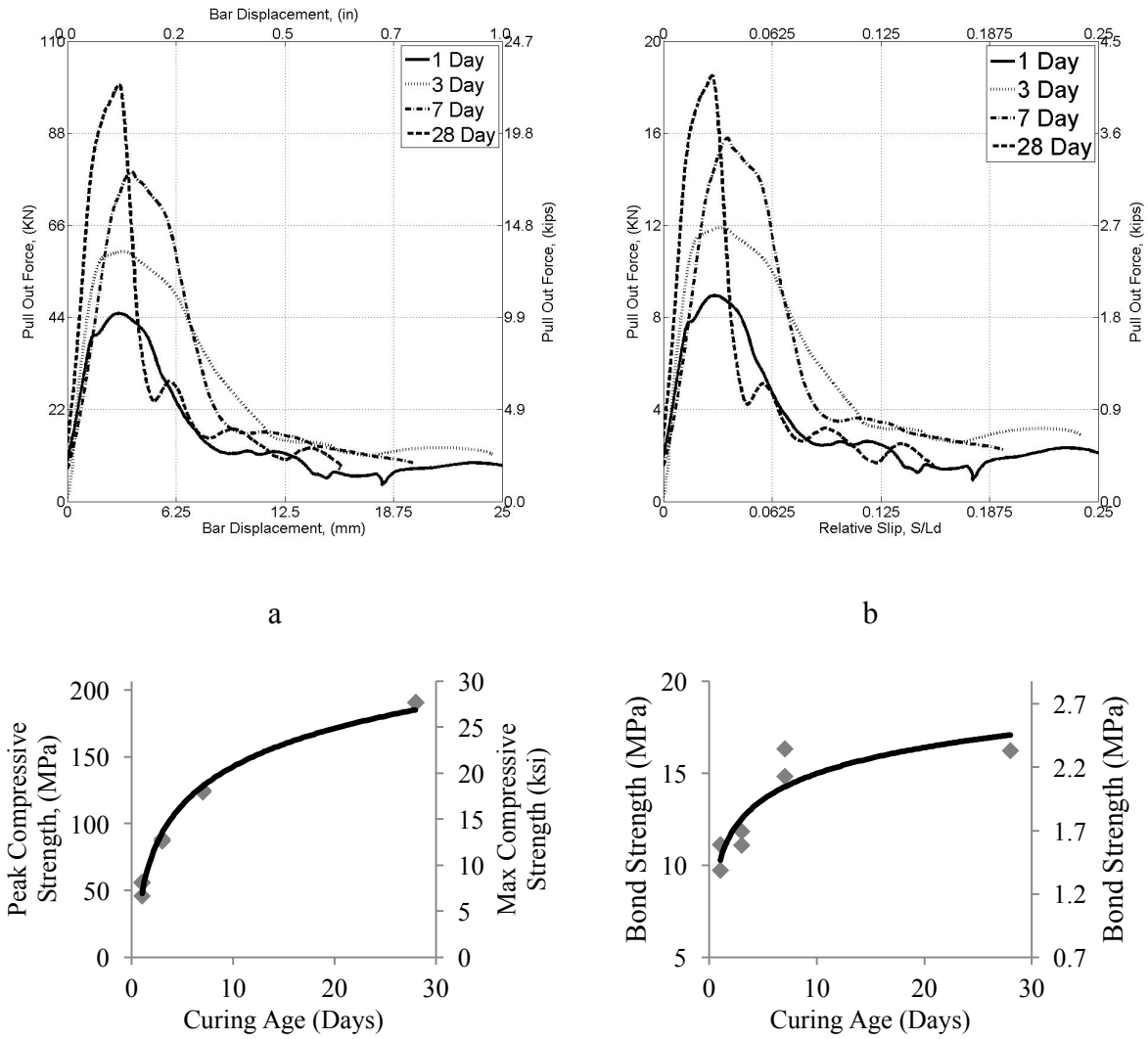

Figure 5-13: (a) Force-Slip Curve, (b) Bond Stress – Relative Slip, (c) Compressive Strength and (d) Bond Stress Data for Early Age Tests

5.2.9. Bar Pull Out vs. Lap Splice Beam Results

As discussed previously, the lap spliced specimens were constructed with the intention of comparing the bond data to that gathered from the simple bar pull out testing. All tests in this series contained #5 (16 mm) dia. bars. Pulls out tests in this configuration were embedded 100 mm, and the UHPC joints had an embedment of 4” (100 mm) and splice lengths of 3.6” (90 mm). Both UHPCs were tested at 1% and 2% fibers by volume. More details regarding the

specimen details, loading and detailed results can be found in Chapter 6. For brevity, only the results are displayed here (Table 5-3). Figure 5-14 lists the average bond stress achieved between the two series of specimens. At 2% fibers by volume, simple bar bull out specimens averaged bond stresses of 2.6 ksi (18.0 MPa), or about 12% more than the 2.3 ksi (15.7 MPa) achieved by the lap-spliced bars. For specimens containing 1% fibers by volume, specimens developed average bond strength 7% less in the lap splice vs. the pull out case. For both of these fiber volume contents, the decrease in strength sits within the current ACI (and AASHTO) limit of an increase of 1.3 l_d increase for lap spliced anchorages. Therefore, increasing simple bar test bond data by the factor prescribed by ACI (and AASHTO) is deemed acceptable for future designs of reduced UHPC anchorage lengths, albeit on the conservative side.

Test		Embedded Length	Splice Length	Force at Joint	Bond Stress
		inches (mm)	inches (mm)	kips	ksi
1	Flexure 1%	4” (100)	3.6” (90)	4.3	2.1
2	Flexure 1%	4” (100)	3.6” (90)	4.3	2.1
3	Flexure 2%	4” (100)	3.6” (90)	4.6	2.2
4	Flexure 2%	4” (100)	3.6” (90)	4.8	2.3

Table 5-3: Test Results Beam Lap Splice Tests

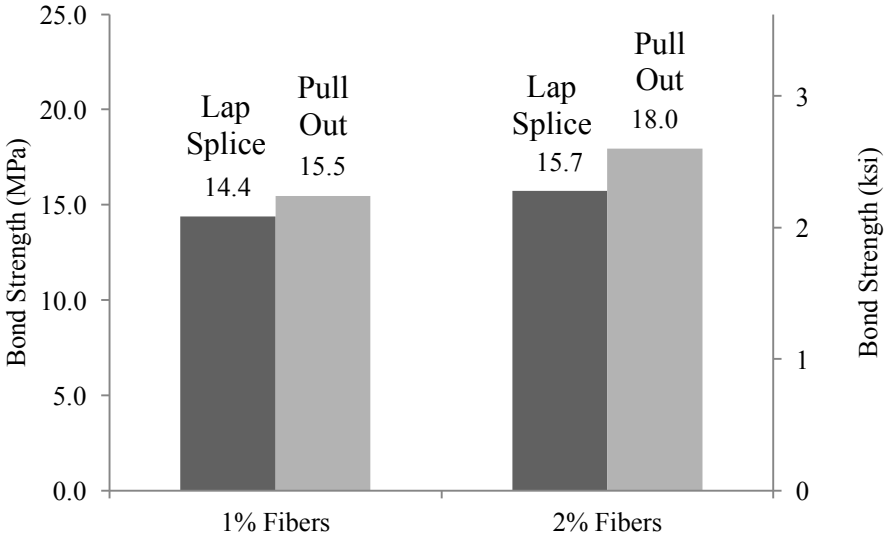

Figure 5-14: Average Bond Stresses in lap splices vs. bar pull out specimens.

5.2.10. Design Implications

Figure 5-15 shows the developed bar stress as a result of the bar coating, embedded length and bar size. The bar stress versus embedment length trend approximately follows the familiar linear relationship seen in other concretes. The data is synthesized into Equation 5-1, which can be used for estimating development lengths in UHPC. The recommendations are for the generic UHPC mix used in this study (Table 5-2), containing 2% fibers by volume and A615 grade 60 epoxy-coated and non-coated (black) bars.

$$\sigma_b = \Upsilon_{\text{config}}(23d_b + 185 + \Psi_c + \Psi_s)$$

$$\Psi_c = \begin{cases} 10 \; for \; Black \; Bar \\ 0 \; for \; Epoxy \; Bar \end{cases} \quad \Psi_s = \begin{cases} 220 \; for \; 13 \; mm \; bar \\ 110 \; for \; 16 \; mm \; bar \\ 0 \; for \; a \; 19 \; mm \; bar \end{cases} \quad \Upsilon_{\text{config}} \begin{cases} 1.0 \; for \; Simple \; Pull \; Out \\ 0.85 \; for \; Lap \; Spliced \end{cases}$$

Equation 5-1: Bar Stress as a function of Embedded Length

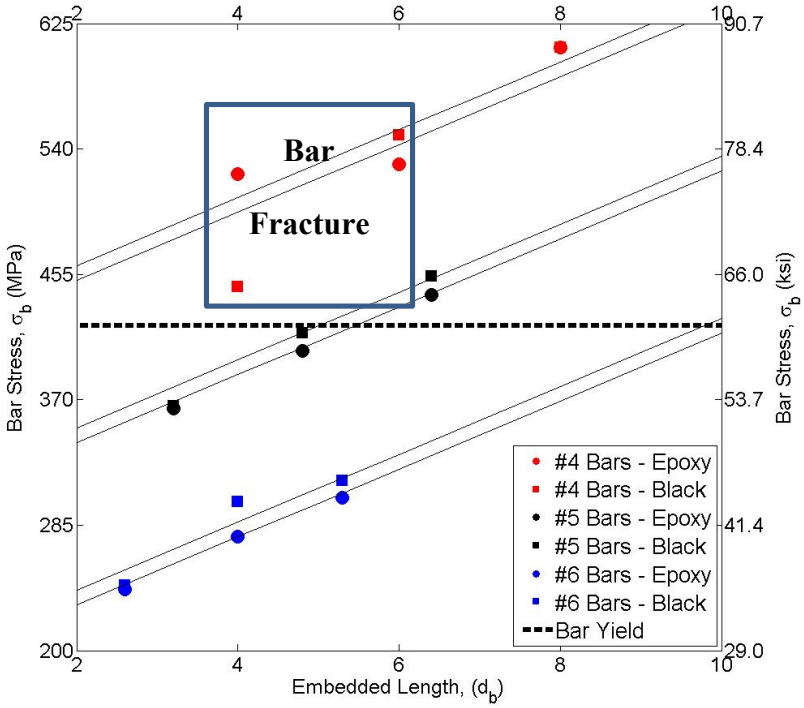

Figure 5-15: Maximum Average Bar Stress under Direct Pull Out

Where d_b is the embedded length of the bar in terms of the bar diameter, Ψ_c is the coating factor, and Ψ_s is the bar size factor. A factor of 15% accounts for the differences in bar force achieved in a pull out test vs. the lap spliced tests. This equation remains limited in scope. Future research plans to determine a more comprehensive relationship including bar cover, fiber content and other parameters.

5.3. CONCLUSION

The objective of this chapter was to investigate the bonding ability between non-proprietary UHPC and steel reinforcement bars. Simple bar pull out tests were performed at 3 different

embedment lengths, 2 bar coatings, 3 bar diameters, 2 fiber volume percentages, and 2 UHPC casting orientations. Early age bonding of UHPC was also tested at 1, 3 and 7 days. Additionally, 4 precast beams were joined together with a UHPC lap splice in order to compare the bonding between the simple pull out case and a more realistic anchorage scenario as well as the effect of fiber content.

- The bond stresses achieved in the simple bar pull out tests ranged from 1.13 ksi (7.8 MPa) to 4.8 ksi (33.1 MPa). At the lower limits of embedment lengths, increasing embedment leads to a reduction in the average bond stress achieved. This is attributed to an uneven distribution of force along the length of the bar, a fact that is established for high strength concretes. A recent series of tests on UHPC, albeit differing in set up and materials used, shows different trends than the data in this study, which suggests that additional investigations in this area are needed.
- Casting the UHPC with the alignment of the fibers transverse to the reinforcement steel showed negligible differences in bonding and strength. More testing should be done to investigate casting effects at a larger scale.
- Changes in steel fiber content by volume resulted in differences between 21% and 36% in bond strength achieved. This is due to reduced concrete strength at lower fiber contents and lower confinement provided.
- Lap spliced joints with UHPC containing 1% fibers by volume achieved just 8% less bond strength than those containing 2% fibers by volume. Since the cost of UHPC strongly depends on the fiber content, these results suggest that structural applications of UHPC with lower fiber volume contents (i.e. cheaper versions of UHPC) should be more

extensively investigated in the future. Most current applications of UHPC entail the use of 2% or more of fibers by volume.

- Bond stresses in the simple bar pull out case were 12% higher than those observed in the lap spliced joints. This value currently falls within the current ACI design limits, making the current standards acceptable for future UHPC embedment design work. Since the result is based on a limited number of specimens and rather conservative, additional research is needed to confirm and refine it.

Intentionally left blank